Superdeformed nuclei

R.V.F. Janssens, T.L. Khoo

SUPERDEFORMED NUCLEI

Robert V. F. Janssens and Teng Lek Khoo

Argonne National Laboratory, Argonne, Illinois 60439, USA

Résumé: Le texte ci-après présente une revue des progrès les plus récents accomplis dans le domaine de l' étude de la superdéformation. L' accent principal est mis sur la présentation des resultats expérimentaux. Parmi les sujets traités on trouvera: (1) la découverte d' une nouvelle région de superdéformation proche de A=190, (2) la surprenante présence de bandes superdéformées avec des transitions identiques en énergie dans des noyaux voisins proches de A=150 et A=190, (3) le rôle de la déformation octupolaire dans le potentiel superdéformé et (4) une discussion des propriétés associées avec l' alimentation et la désexcitation des bandes superdéformées. Ce texte apparaitra comme une contribution à la revue Annual Review of Nuclear and Particle Science, Volume 41.

Abstract: This paper reviews the most recent advances in the understanding of the physics of superdeformed nuclei from the point of view of the experimentalists. It covers among other subjects the following topics: (1) the discovery of a new region of superdeformed nuclei near A=190, (2) the surprising result of the occurrence of bands with identical transition energies in neighboring superdeformed nuclei near A=150 and A=190, (3) the importance of octupole degrees of freedom at large deformation and (4) the properties associated with the feeding and the decay of superdeformed bands. The text presented hereafter will appear as a contribution to the Annual Review of Nuclear and Particle Science, Volume 41.

1. INTRODUCTION

The ever increasing accuracy with which nuclear structure studies can be performed experimentally and theoretically has yielded a wealth of fascinating new results. It is by now well known that throughout the periodic table, nuclei can adopt a rich variety of shapes, particularly when rotated. This is the result of the interplay between macroscopic (liquid drop) and microscopic (shell correction) contributions to the total energy of the nucleus. The shell correction is a quantal effect arising from the occupation of non-uniformly distributed energy levels. Rotation affects the nuclear shape by modifying both the liquid drop moment of inertia and the nucleonic occupation of specific shape-driving orbitals. Many interesting phenomena have been reported in rapidly rotating nuclei; examples are the alignment of particle spins along the rotation axis (backbending), the transition from prolate collective to oblate aligned-particle structures (band termination), the possible occurrence of triaxial shapes, and the onset of octupole instabilities. The most spectacular experimental result to date is the discovery of superdeformation, where nuclei are trapped in a metastable potential minimum associated with very elongated ellipsoidal shapes corresponding to an axis ratio of roughly 2:1.

Superdeformation was first proposed some twenty years ago to explain the fission isomers observed in some actinide nuclei [1,2]. It was later realized that superdeformed shapes can occur at high angular momentum in lighter nuclei [3-7]. The interest in the mechanisms responsible for these exotic shapes has increased enormously with the discovery of a superdeformed band of nineteen discrete lines in ^{152}Dy [8]. At about the same time, evidence for highly deformed nuclei (axis ratio 3:2) was also reported near ^{132}Ce [9]. Striking properties emerged from the first experiments, such as the essentially constant energy spacing between transitions ("picket-fence" spectra), the unexpectedly strong population of superdeformed bands at high spins, and the apparent lack of a link between the superdeformed states and the yrast levels.

These findings were reviewed by Nolan and Twin [10]. The present article follows upon this work and discusses the wealth of new information that has since become available. This includes the discovery of a new "island" of superdeformation near A = 190, the detailed spectroscopy of "ground" and excited bands in the superdeformed well near A = 150 and A = 190, the surprising occurrence of superdeformed bands with identical transition

energies in nuclei differing by one or two mass units, and the improved understanding of mechanisms responsible for the feeding into and the decay out of the superdeformed states.

2. A NEW REGION OF SUPERDEFORMATION

2.1 Calculations of Superdeformed Shapes

As alluded to above, the single-particle energy spectrum plays an essential role in the determination of the nuclear shape. The stability of spherical nuclei at closed shells is related to large gaps in the energy level spectrum of the various orbitals. Shell gaps also occur in the single-particle spectrum for specific deformations. In an axially symmetric harmonic oscillator [11], these shell gaps occur when the lengths of the principal axes form integer ratios and, in particular, when the ratio is 2:1:1, which corresponds to a quadrupole deformation β_2 [12] of 0.65. These shell corrections, superimposed on a smooth liquid drop contribution, can generate local minima in the potential energy surface. The cranked-Strutinsky method is often used to calculate potential energy surfaces. In this approach, the total energy of a nucleus is calculated as a sum of liquid drop and shell correction terms. The liquid drop energy is a sum of Coulomb, surface and rotational energies. All of these terms are calculated as a function of nuclear deformation. In the heaviest nuclei, strong Coulomb forces favor large deformations, balancing the surface energy which favors compact shapes. Because of this balancing, shell corrections at large deformations give rise to pronounced potential minima which are responsible for the fission isomers [1]. At high spin in the A = 150 region, it is the rotational energy term that balances out the surface term at large deformation and makes superdeformation possible. Several cranked-Strutinsky calculations, using either an anharmonic oscillator potential [5,13] or a Woods-Saxon potential [6,7], have been quite successful in predicting the existence of an "island" of superdeformation for $Z \sim 64$ and $N \sim 86$ as well as the occurrence of "nearly" superdeformed nuclei ($\beta_2 = 0.4$) for $Z \sim 58$ and $N \sim 74$. The calculations indicate that pronounced secondary minima are obtained only when both proton and neutron shell corrections are favorable and this leads to the occurrence of these "islands" in the periodic table.

Superdeformed minima in a great number of nuclei with $Z \geq 80$ were originally predicted by Tsang and Nilsson [3] at zero spin and later confirmed

in several other calculations. From general expectations (e.g. ref. [5]), these minima survive and come closer to the yrast line with increasing spin. More recent calculations [13-15] have suggested that the superdeformed minimum becomes yrast at spins in excess of 30$\hbar$ in nuclei with Z ~ 80, N ~ 112. Calculated potential energies [15] as a function of quadrupole deformation are presented in fig. 1 for different spin values in the nucleus ^{191}Hg. From the figure, it is clear that a deep minimum exists at very large deformation (β_2 ~ 0.5, axis ratio ~ 1.65:1) and this minimum is calculated to persist down to the lowest spins even though the well depth diminishes. Here, both strong Coulomb and rotational effects play a significant role. The occurrence of a superdeformed minimum at zero spin in the A = 190 region has also been predicted in calculations using static, self-consistent Hartree-Fock and Hartree-Fock-Bogoliubov calculations [16,17].

2.2 The First Superdeformed Band in the A = 190 Region

First experimental evidence for a new region of superdeformation near A = 190 became available in 1989. As can be seen in figure 2, a weak rotational band of 12 transitions was observed in the nucleus ^{191}Hg [18]. The measured properties of this band identify it as a superdeformed band; i.e. (1) the average energy spacing is small (37 keV) and corresponds to an average dynamic moment of inertia $J^{(2)}$ of 110 $\hbar^2$MeV^{-1}, which agrees well with expectations based on cranked-Strutinsky calculations [15], and (2) the measured average quadrupole moment of 18 $\pm$ 3 eb implies a large quadrupole deformation (β_2 ~ 0.5). The band also exhibits other characteristics which are similar to those noted for superdeformed bands in the A = 150 region, such as (1) the small total intensity with which the band is fed (the flow through the band represents ~2% of the ^{191}Hg intensity), (2) the intensity pattern (which shows that γ-ray intensity in the band decreases gradually with increasing γ-ray energy, while at the bottom of the cascade it remains constant over the last 3-4 transitions), and (3) the fact that the transitions linking the superdeformed band to the yrast states could not be observed.

Several important questions were raised by the original experimental result. First, $J^{(2)}$ was found to increase steadily with the rotational frequency $\hbar\omega$ (defined as $E_\gamma/2$). Mean-field calculations which attempt to reproduce variations in $J^{(2)}$ have suggested that such a rise may be attributed to three major factors which could contribute separately or cooperatively: (i) shape changes as a function of $\hbar\omega$ (e.g. centrifugal

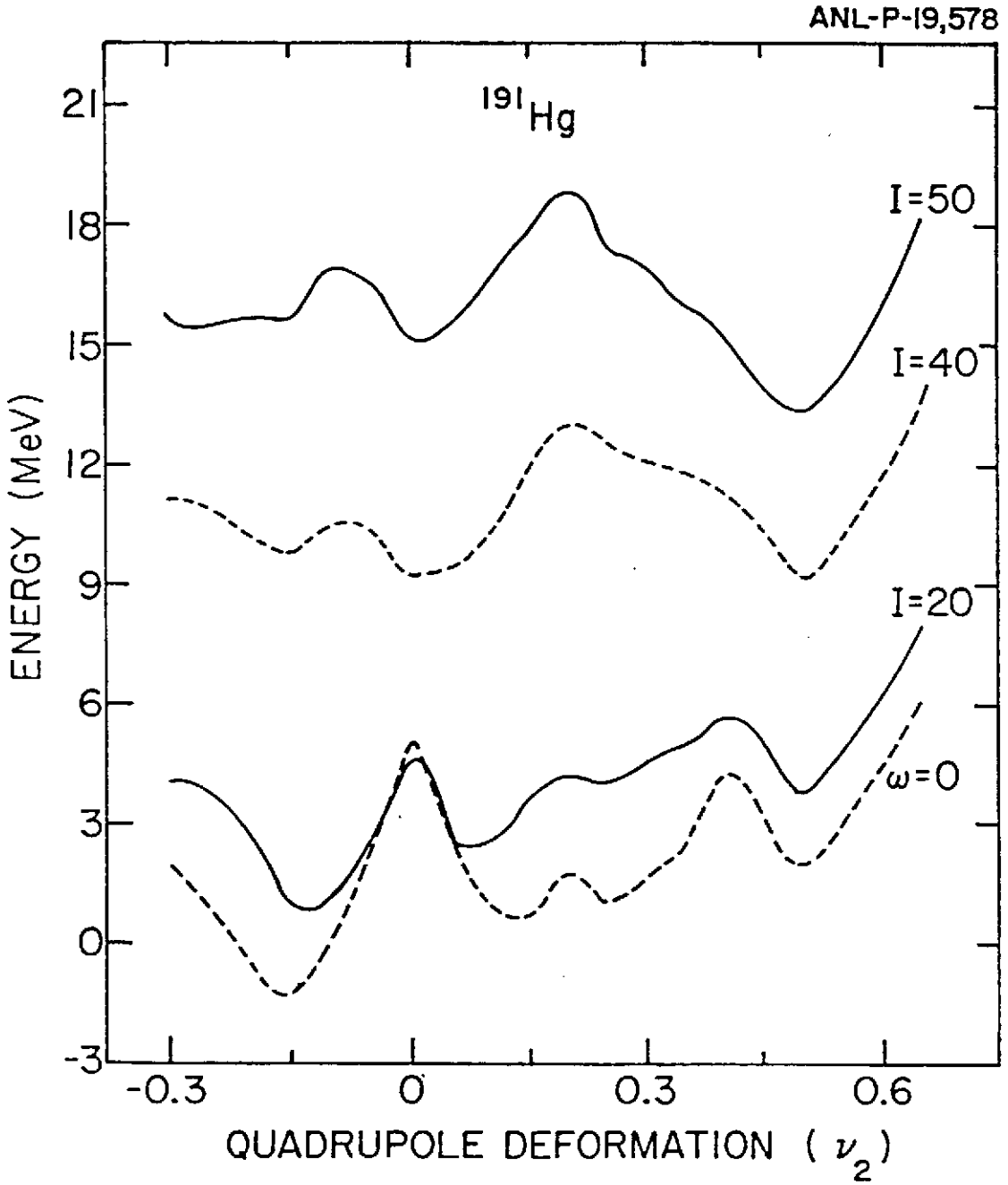

Figure 1: Total energy as a function of quadrupole deformation for different spin values in ^{191}Hg (from [15]).

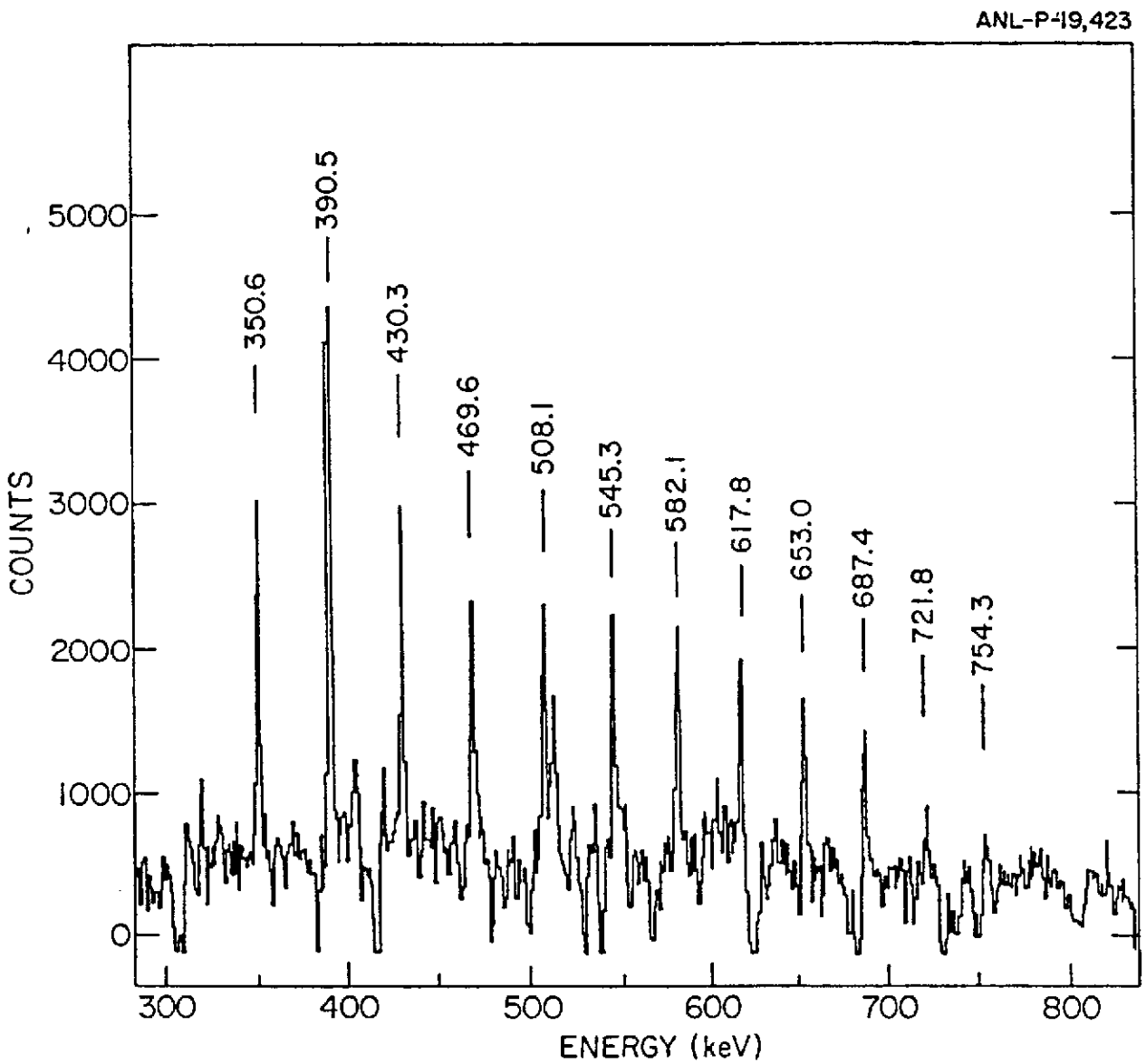

Figure 2: γ-ray spectrum of the first superdeformed band observed in the A = 190 region [18]. The 390 keV transition is an unresolved doublet consisting of a transition in the superdeformed band and the $17/2^+$-$13/2^+$ groundstate transition in ^{191}Hg.

stretching), (ii) changes in pairing at large deformations [19], and (iii) occupation of specific high-N orbitals [19,20] (i.e. high-N orbitals from two major shells higher which plunge down as a function of deformation and come towards the Fermi surface at very large deformations, in this case $i_{13/2}$ protons and $j_{15/2}$ neutrons). Second, this superdeformed band was found to decay only to the $17/2^+$ yrast state of ^{191}Hg, and it was neither possible to obtain a firm indication of the spins of the superdeformed states nor to assess whether the link between superdeformed states and the yrast levels is statistical in nature, as in the A = 150 region [10], or occurs only through a few specific transitions. Finally, questions concerning the existence of other superdeformed nuclei (as predicted by theory [15]) and the limits in N and Z of the superdeformed region also needed attention.

2.3 Superdeformation in ^{192}Hg

An impressive number of new results in the A = 190 region has become available recently. However, before presenting these we shall first summarize the present experimental situation concerning ^{192}Hg, the nucleus regarded as the analog of ^{152}Dy for this region in the sense that shell gaps are calculated [15,21] to occur at large deformation for both Z=80 and N=112 (see below). The superdeformed band of ^{192}Hg, measured with the ^{160}Gd(^{36}S,4n) reaction at 162 MeV [22], is presented in fig. 3a. (The 16 transitions have also been observed in an independent experiment [23].) The total flow through the band represents 1.9% of all transitions in ^{192}Hg. From fig. 3a it is clear that the band feeds the known levels up to 8^+ in the positive-parity yrast sequence and up to 9^- in the negative parity band. Transitions which link the superdeformed band with known yrast levels could not be found. It is likely that many different decay paths share the intensity and that the link is statistical in nature. This assumption is supported by the observation that the feeding into the yrast states is spread over several states belonging to bands of opposite parity with rather different intrinsic structure [24]. Thus, the mechanism of deexcitation out of the superdeformed bands in this region appears to be similar to that discussed for the A = 150 region [10].

As in the case of ^{191}Hg, the transition energies in the superdeformed band of ^{192}Hg extend to much lower energy than in superdeformed bands of the A = 150 region (the lowest transition energy in ^{152}Dy is 602 keV, as opposed to 257 keV in ^{192}Hg). If transition energies (and rotational frequencies) can be related to spin, this result indicates that superdeformation persists to lower

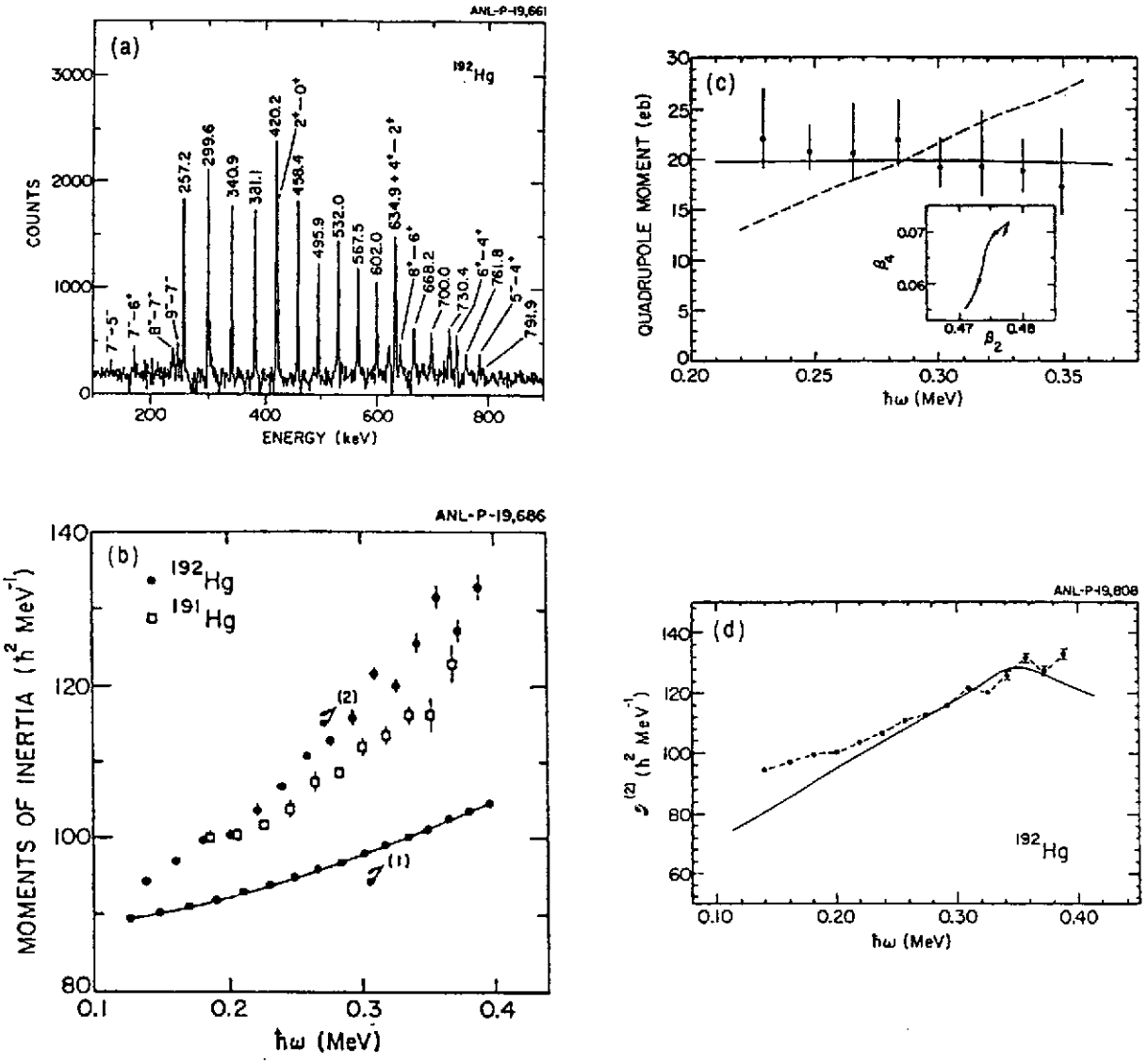

Figure 3: (a): spectrum of the superdeformed band in ^{192}Hg obtained from the sum of selected coincidence spectra [22]. The energies of the superdeformed transitions are indicated and transitions between yrast states are also given.
(b): comparison between the dynamic moments of inertia $J^{(2)}$ for the superdeformed bands in ^{191,192}Hg. The static moment of inertia $J^{(1)}$ is also given for ^{192}Hg assuming spin values for superdeformed states discussed in the text.
(c): comparison between the measured and calculated transition quadrupole moments Q_t in the superdeformed band of ^{192}Hg [25]. The dashed line represents a calculation assuming that the rise in $J^{(2)}$ is due to centrifugal stretching, the solid line is the result of a cranked shell model calculation discussed in the text and the inset shows the calculated change in the deformation parameters over the frequency range of interest (the arrows point towards increasing frequency).
(d): comparison between the measured and calculated $J^{(2)}$ values for the superdeformed band in ^{192}Hg [25].

spin in the new region. The data on ^{192}Hg allow for the verification of this assertion. The spin of the lowest level in the superdeformed band was estimated to be 10$\hbar$ from the average entry spin (8$\hbar$) into the yrast states [22,23] and the assumption of a $\Delta\ell$=2$\hbar$ angular momentum removal by the transitions linking the superdeformed states and the yrast line. The same spin value is also obtained [23] from a procedure where $J^{(2)}$ is fit by a power series expansion in ω^2, which is then integrated to give the spin (see section 4.2). With these assumed spin values, a static moment of inertia $J^{(1)}$ can be derived: the latter is presented as a function of $\hbar\omega$ together with the values of $J^{(2)}$ in fig. 3b. It is striking that: (1) there is a large monotonic increase (40%) in $J^{(2)}$ with $\hbar\omega$, (2) the $J^{(2)}$ values for ^{192}Hg are similar, but always higher than those for ^{191}Hg at the same frequency, and (3) $J^{(2)}$ is significantly larger than $J^{(1)}$ for all values of $\hbar\omega$.

Crucial information regarding the properties of the ^{192}Hg superdeformed band were provided by detailed measurements of lifetimes with the Doppler-shift attenuation method (DSAM) [25]. In contrast with previous measurements for superdeformed states, where only fractional Doppler shifts $F(\tau)$ were reported [10,18], in this work one has been able to analyze detailed lineshapes for individual transitions between superdeformed states. Such an analysis allows one to determine the variation of transition quadrupole moment (Q_t) as a function of $\hbar\omega$, as opposed to previous studies where Q_t was assumed to be constant for all states in the band. The measured lifetimes τ were transformed into transition quadrupole moments $Q_t(I)=(1.22<I020/I-2>^2\tau E_\gamma^5)^{-1/2}$ assuming the spin values given above. The Q_t-values are displayed as a function of $\hbar\omega$ in fig. 3c. As can be seen, the quadrupole moment Q_t, and hence the deformation, remain essentially constant ($Q_t \sim 20 \pm 2$ eb) over the entire frequency range. This result rules out centrifugal stretching as an explanation for the rise in $J^{(2)}$: this is illustrated by the dashed line in fig. 3c, where the values of Q_t have been derived assuming that the change in $J^{(2)}$ is entirely due to a variation in deformation.

Bengtsson et al [20] have shown that the occupation of specific high-N intruder orbitals plays an important role in understanding the variations of $J^{(2)}$ with mass number and rotational frequency in the A = 150 region. This effect alone cannot account for the variation in $J^{(2)}$ in ^{191,192}Hg: mean-field calculations without pairing, such as those by Chasman [15] or Åberg [13], give proton and neutron contributions to $J^{(2)}$ which remain essentially

constant with $\hbar\omega$. This finding points to the need to examine the effects of pairing (possibility (ii) in the discussion above) as pointed out originally by Ye et al [22]. This is best done in the framework of cranked deformed shell model calculations which include the effects of static and dynamic pairing, using either the Woods-Saxon or the modified-oscillator approach. The basis for these calculations is discussed in detail in refs. [26,27] and the first applications to the Hg nuclei can be found in refs. [21,25,28,29]. The neutron and proton Woods-Saxon routhians for large deformation [21] are presented in figure 4. It is seen that the large Z=80 shell gap remains at all rotational frequencies. In the neutron system there are two single-particle gaps at N=112 and N=116, separated by two high-K levels [512]5/2 and [624]9/2. Because of these shell gaps, $^{192}_{80}Hg_{112}$ can be regarded as a doubly magic nucleus in the superdeformed well. For this nucleus the relevant high-N intruder orbitals which are occupied in the superdeformed configuration are four ($i_{13/2}$) protons and four ($j_{15/2}$) neutrons. Adopting the nomenclature of Bengtsson et al [20], the superdeformed configuration in ^{192}Hg can be labelled ($\pi 6^4 \nu 7^4$). Figure 3d compares the calculated dynamic moment of inertia with the data. In the calculation, pairing correlations were treated self-consistently by means of the particle number projection procedure [26], but the neutron pairing interaction strength was reduced. The rise in the calculated $J^{(2)}$ can be ascribed to the combined gradual alignment of a pair of N=6 ($i_{13/2}$) protons and of a pair of N=7 ($j_{15/2}$) neutrons within the frequency range under consideration. The data are reproduced rather well. The evolution of the nuclear shape with $\hbar\omega$ was also calculated. The inset in fig. 3c illustrates that within the frequency range of interest the predicted changes in the β_2 and β_4 deformation parameters are very small. The resulting Q_t-values agree well with the measured values as is shown by the solid line in fig. 3c. The success of the calculations in reproducing all aspects of the data allows one to propose that quasiparticle alignments and the resulting changes in pairing represent a major factor contributing to the rise in $J^{(2)}$ in ^{192}Hg and, probably, in other nuclei in this region. Further evidence for this conclusion, as well as for the power of the calculations, is discussed below.

2.4 Neutron and Proton Excitations in the Superdeformed Minimum

Figure 5 presents the dynamic moments of inertia of all the superdeformed bands observed so far in the A = 190 region: bands have been identified in all Hg isotopes with A=189-194 [18,21-23,28,30-33], in ^{193,194}Tl [34,35] and

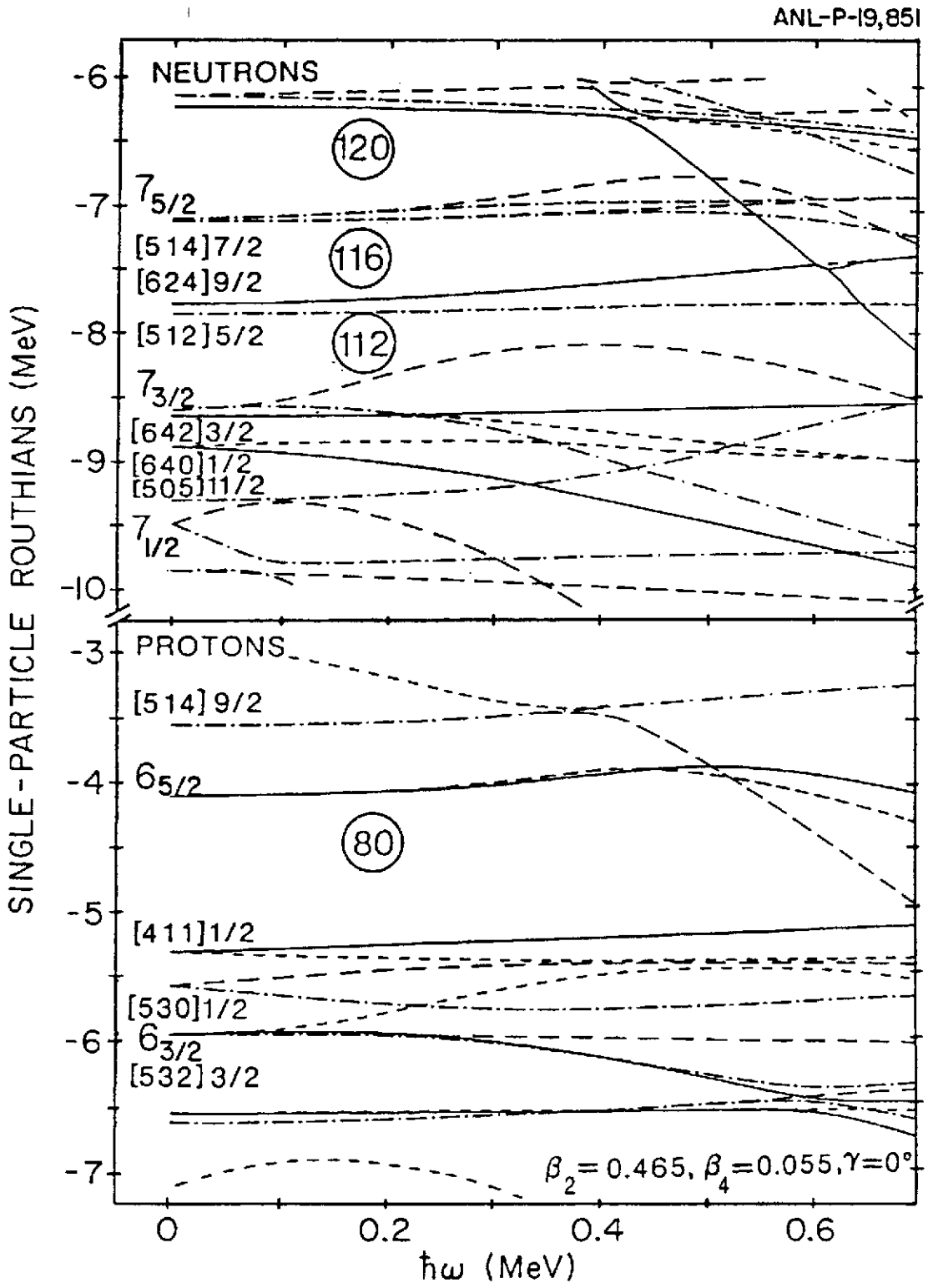

Figure 4: Representative neutron and proton Woods-Saxon routhians for ^{192}Hg. The conventions adopted are given in ref. [28].

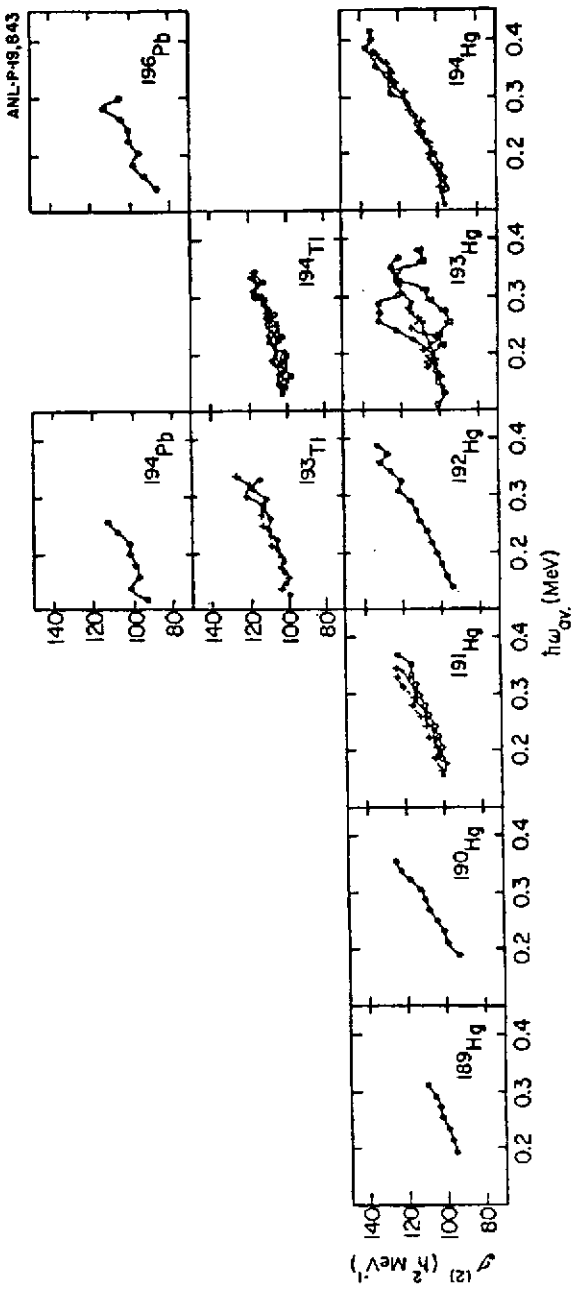

Figure 5: Dynamic moments of inertia $\mathcal{J}^{(2)}$ as a function of rotational frequency for all superdeformed bands in the A = 190 region. The data are from refs. [18,21-23,28,30-37].

in ^{194,196}Pb [36,37]. Furthermore, in many nuclei several superdeformed bands have been reported. Thus, just as in the A = 150 region discussed below, it has been possible to perform detailed spectroscopy in the superdeformed well. Most of the data can be understood in the framework of the cranked shell model calculations with pairing introduced in section 2.3, and specific configurations have been proposed [21,29] for many of the bands of fig. 5. Neutron configurations involving the intruder orbital $7_{3/2}$ and/or the [642]3/2, [512]5/2 and [624]9/2 levels (fig. 4) have been proposed for the superdeformed bands in the Hg isotopes (the proton configuration being always $\pi 6^4$). In ^{194}Hg, for example, the superdeformed yrast band still contains the $\pi 6^4 \nu 7^4$ configuration, but the lowest neutron excitations are predicted to involve promotion from the [512]5/2 to the [624]9/2 levels. This will lead to two pairs of strongly coupled bands with negative parity showing no signature splitting. Three superdeformed bands have been observed in this nucleus [21,33]. Their properties match the expectations: the two excited bands are interpreted as one signature partner pair, since the γ-ray energies in one of the bands are observed to lie mid-way between those of the other within 1 keV over the entire frequency range, and both bands are of similar intensity. Equally successful comparisons between the data and the calculations can be made for the bands of the other Hg isotopes. The only noticeable exception is the case of ^{193}Hg where some of the observed features [32], such as the irregularities in the evolution of $\mathcal{J}^{(2)}$ with $\hbar\omega$ for two of the bands (fig. 5), cannot be readily understood within the framework of the calculations. The suggestion has been made that octupole effects have to be taken into account. This is discussed in section 5.

The cranked shell model calculations with pairing appear to be equally successful in the case of proton excitations. Considering the proton routhians of fig. 4, the [411]1/2, [530]1/2 and [532]3/2 levels are important for superdeformed nuclei with $Z \lesssim 80$, while the third $i_{13/2}$ ($6_{5/2}$ in fig. 4) intruder orbital and the [514]9/2 state should characterize superdeformed bands in the Tl and Pb nuclei. At present, no superdeformed bands have been observed in the Au or Pt nuclei, and it is possible that this observation underlines the importance of the Z=80 shell gap. On the other hand, superdeformed bands have been seen in several Pb and Tl nuclei [34-37]. In ^{193}Tl, for example, the yrast superdeformed configuration is labelled as $\pi 6^3$ in the calculations, and exhibits some signature splitting at $\hbar\omega \geq 0.2$ MeV (fig. 4), leading to the expectation that two signature partner bands should be observed: this is the case experimentally [34]. A direct

comparison of the $J^{(2)}$ values for ^{193}Tl with those observed in ^{192}Hg and in the first ^{191}Hg superdeformed band (which, as ^{193}Tl, is thought to contain a single nucleon in a high-N intruder orbital) is also particularly revealing (fig. 6). The occupation of the third $i_{13/2}$ orbital in ^{193}Tl results in an increase in the value of $J^{(2)}$ with respect to ^{192}Hg at the lowest frequencies. In both ^{191}Hg and ^{193}Tl, $J^{(2)}$ is essentially constant at the lowest frequencies before exhibiting the characteristic rise described above. This feature is also present in the calculations and is proposed to be a signature for the occupation of these high-j intruder orbitals by a single nucleon [34]. In the ^{191}Hg band, the alignment of the $j_{15/2}$ neutron is blocked and the rise in $J^{(2)}$ is attributed to the alignment of the $i_{13/2}$ protons while in ^{193}Tl the opposite situation occurs. The fact that the rise in $J^{(2)}$ with $\hbar\omega$ is very similar in both cases implies that neutron and proton alignments have contributions of comparable magnitude. Furthermore, the rise of $J^{(2)}$ in ^{193}Tl starts at lower frequency than that in ^{191}Hg. This suggests that the neutrons align at somewhat lower frequency than the protons, in agreement with the calculations.

From the discussion above, it can be concluded that a good description of the superdeformed bands within the framework of cranked shell model calculations with pairing can be achieved. Two points need, however, to be emphasized. First, the transition energies in some of the superdeformed bands are surprisingly close to those of bands in neighboring nuclei and several bands can be related to ^{192}Hg [40]. This property is discussed in section 4. Second, the inclusion of pairing is crucial for reproducing the data and, in particular, the smooth increase of $J^{(2)}$ with $\hbar\omega$. In the proton system, pairing is reduced by the presence of the Z=80 shell closure. As was shown in refs. [21] and [28], the calculations require that the neutron pairing be reduced as well if one wants to reproduce the similarities in the behavior of $J^{(2)}$ with $\hbar\omega$ observed in <u>all</u> nuclei in this region. Reduced pairing is to be expected on the basis of general arguments [38]. Pairing is sensitive to the overlap between orbitals of interest. At the very large deformations being considered here, states originating from different shells approach the Fermi level, and these states will only be very weakly coupled through the pairing interaction. Moreover, the coupling between the all important unique-parity levels (i.e. the various components of the high-N intruders) is also severely reduced because of their sizable energy splitting at large deformation. First attempts to provide a quantitative estimate of the reduction in pairing are discussed in refs. [38,39].

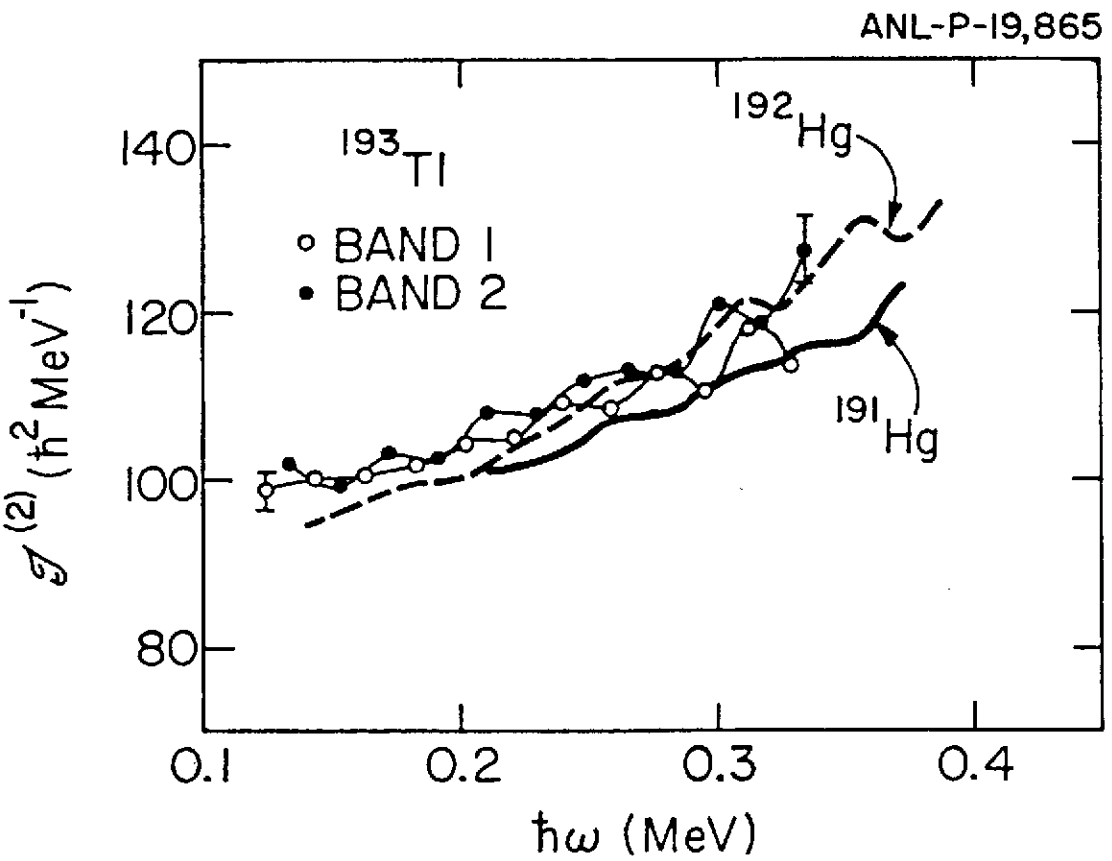

Figure 6: Comparison between the dynamic moments of inertia $J^{(2)}$ measured in the superdeformed bands of ^{193}Tl, ^{192}Hg and ^{191}Hg (yrast superdeformed band). The data are from refs. [22,28,34].

3. SUPERDEFORMATION IN THE A = 150 REGION: "IDENTICAL" BANDS

3.1 High-N Orbital Assignments in the Superdeformed Minimum

Since the review by Nolan and Twin [10], where the two first superdeformed bands of the A = 150 region were discussed (^{152}Dy and ^{149}Gd), the "island" of superdeformed nuclei in this mass region has expanded considerably. Superdeformed bands have now been identified in all Gd isotopes with A=146-150 [41-46], in ^{150,151}Tb [44,45,47], as well as in $^{151-153}$Dy [8,48,49]. Furthermore, in many cases several superdeformed bands have been seen in the same nucleus: a summary of the available data on the $\mathcal{J}^{(2)}$ moments of inertia is presented in fig. 7. Preliminary reports of similar band structures in ^{145}Gd and ^{142}Eu have also become available [50,51]. As in the A = 190 region, differences in the variations of $\mathcal{J}^{(2)}$ with $\hbar\omega$ from nucleus to nucleus have been attributed to the occupation of specific high-N intruder orbitals. In the A = 150 region, $^{152}_{66}Dy_{86}$ can be described as the "doubly magic" nucleus: all available calculations indicate the presence of very large shell gaps at Z=66 and N=86 for a quadrupole deformation $\beta_2 \sim 0.6$. The occupation of specific high-N intruder orbitals can have dramatic effects: in the case of the Dy isotopes for example, $\mathcal{J}^{(2)}$ is seen to rise smoothly over the entire frequency range in ^{151}Dy (fig. 7), while a smooth decrease is seen in ^{152}Dy and an essentially constant value of $\mathcal{J}^{(2)}$ is observed for the yrast superdeformed band in ^{153}Dy (it is assumed that the most intensely populated band is the "ground" band in the second well). For these isotopes, the proton contribution has been assigned as $\pi 6^4$ (i.e. $i_{13/2}$) and the observed differences have been attributed to changes in the occupation of the $j_{15/2}$ neutron orbitals ($\nu 7^1$, $\nu 7^2$ and $\nu 7^3$ for $^{151-153}$Dy, respectively), which result in contributions of varying magnitude to $\mathcal{J}^{(2)}$ [20]. While the calculations of ref. [20] where performed without pairing and at a fixed deformation, more recent Woods-Saxon cranked shell model calculations [19,26] have taken into account small variations of the shape with spin as well as changes in deformation from one nucleus to another. These calculations also treat pairing correlations self-consistently (see also ref. [52] for the treatment of pairing). The best indication for the importance of the inclusion of pairing correlations and shape effects in this mass region comes from the data on the Gd isotopes. In the yrast superdeformed band of ^{150}Gd, for example, $\mathcal{J}^{(2)}$ is not only seen to decrease with $\hbar\omega$, but also exhibits a dramatic fall off at the lowest frequencies (fig. 7). In the calculations, this band is assigned a $\pi 6^2 \nu 7^2$ configuration. This is in agreement with the assignment

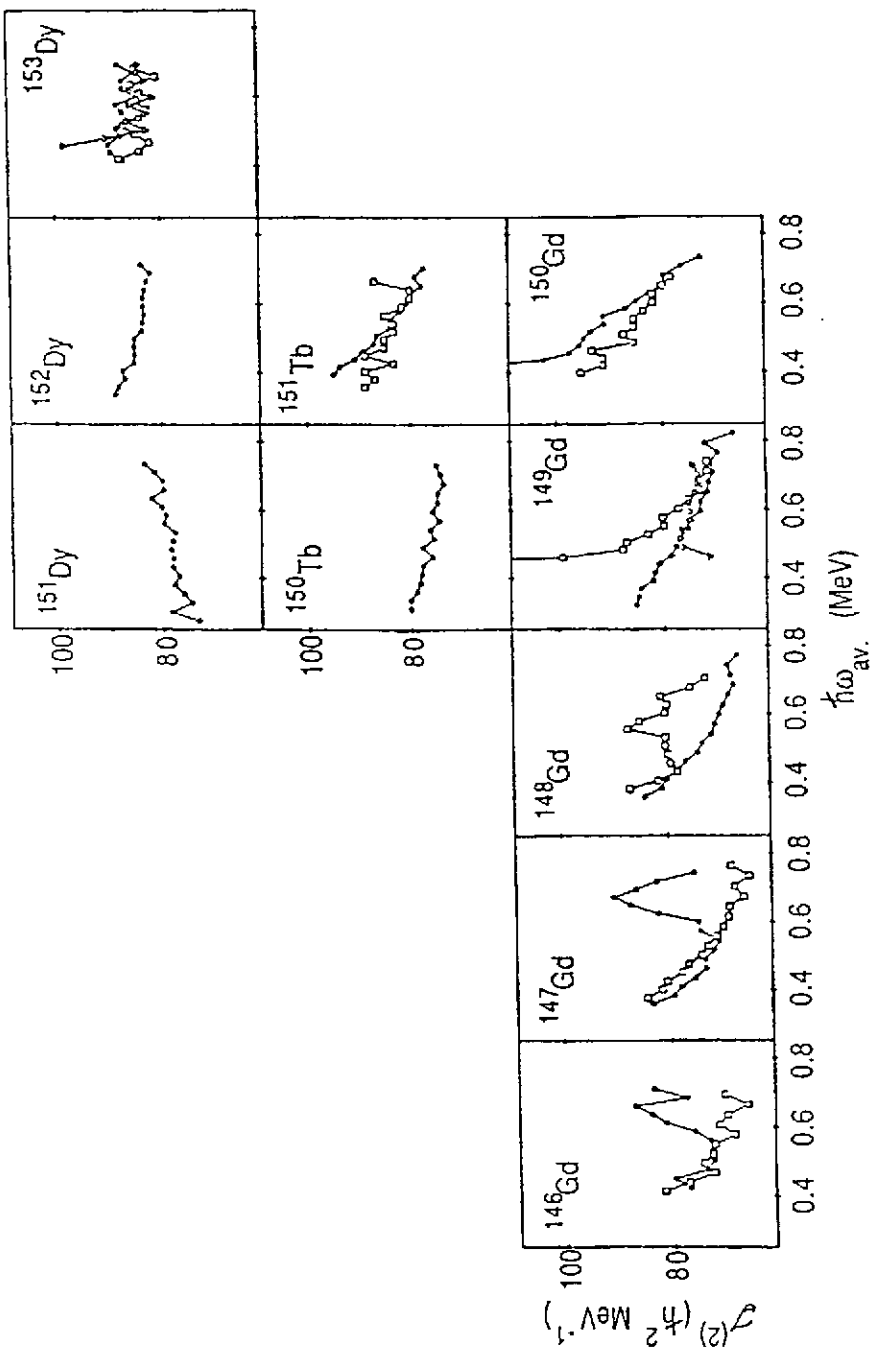

Figure 7: Dynamic moments of inertia $J^{(2)}$ for all superdeformed bands in the A = 150 region. The data are from refs. [8,10,41-49].

of ref. [20], but the alignment of a pair of $j_{15/2}$ neutrons at $\hbar\omega \sim 0.4$ MeV (i.e. a band crossing) has to be invoked to account for the sharp drop in $\mathcal{J}^{(2)}$. The observation that the deexcitation out of the superdeformed band in ^{150}Gd is extremely abrupt, with essentially all the intensity being lost over a single transition, has been interpreted as additional evidence for this band crossing, which in turn requires the presence of the pairing correlations [45]. Marked irregularities in the behavior of $\mathcal{J}^{(2)}$ can also be seen in the yrast superdeformed bands of ^{146,147}Gd as well as in an excited band in ^{148}Gd (fig. 7). At present, there is some argument regarding the exact orbitals involved in these crossings as well as concerning the role of pairing and/or octupole correlations [26,41,42,46]. The general conclusion, however, remains that in all yrast superdeformed bands near A = 150 the variations of $\mathcal{J}^{(2)}$ with $\hbar\omega$ reflect the major role played by the few nucleons in high-N orbitals, and the adopted configurations are $\pi 6^{2,3,4}$ for Gd, Tb, and Dy respectively; $\nu 7^0$ or $\nu 7^1$ for N=82-85; $\nu 7^2$ for N=86 and $\nu 7^3$ for N=87. The number of occupied intruder orbitals varies in some of the excited bands.

3.2 Superdeformed Bands with Identical Energies

The discovery of multiple superdeformed bands within a single nucleus has made it possible to investigate the microscopic structure of both the ground and excited states in the second well. However, a greater impetus for detailed studies of excited bands has been the unexpected discovery that several pairs of related bands have almost identical transition energies. The first reported [53] cases consisted of the pairs (^{151}Tb*, ^{152}Dy) and (^{150}Gd*, ^{151}Tb) - the * denotes an excited superdeformed band - where transition energies in the pair were found to be equal to within 1-3 keV over a span of 14 transitions. Later, another similar pair (^{149}Gd*, ^{150}Tb) was found [44] (the notation ^{149}Gd** is used in ref. [44] as it is suggested that the second excited superdeformed band in ^{149}Gd is involved). This is illustrated in fig. 8 where the difference between "identical" transitions energies ΔE_γ is plotted versus the transition energy. It can be seen that, on average, the deviation is less than 1 keV for the first pair and only slightly larger for the other two. This implies that transition energies are equal to better than 3 parts in 1000. This is a rather surprising equality and is quite unprecedented in nuclear physics! γ-ray energies should scale with the moment of inertia J, which is proportional to $A^{5/3}$ ($J \sim MR^2$), so that adjacent mass nuclei would have energies different by ~14 keV. Furthermore, the spins of corresponding transitions in each pair necessarily differ by $1/2\hbar$, leading

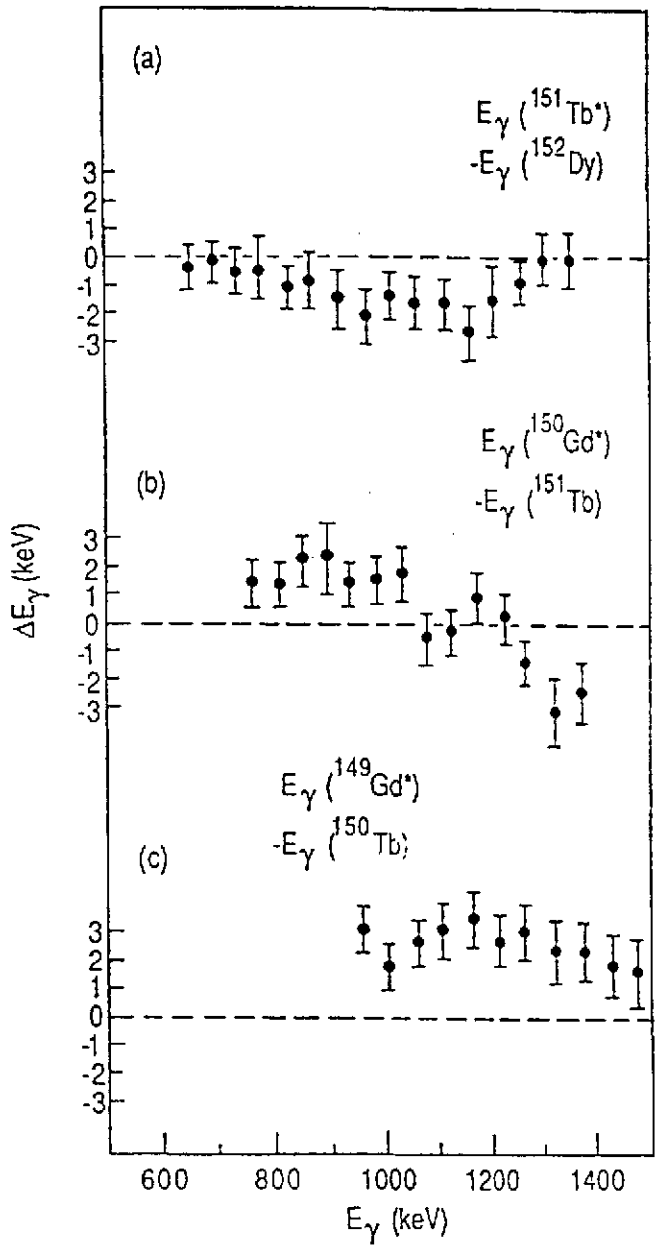

Figure 8: Differences in the γ-ray energies ΔE_γ between the superdeformed bands in (a) (^{151}Tb*, ^{152}Dy), (b) (^{150}Gd*, ^{151}Tb) and (c) (^{149}Gd*, ^{150}Tb). The data are taken from refs. [44,53].

to differences in E_γ of ~13 keV. For (A-1*, A) pairs, with A even, these differences would reinforce each other.

A word of caution is in order since it is assumed that each pair of transitions being compared has the appropriate spins (I+1/2,I), but the spins of the superdeformed bands have not been measured. Since the spacing between consecutive transitions in each band is ~50 keV, the maximum difference in energy in a pair of bands is ~25 keV if no spin correlation is involved. However, with three cases and not just an isolated one, it is unlikely that these degeneracies are accidental. Furthermore, in all three cases the excited (A-1)* superdeformed band is proposed to be characterized by a hole in the same specific orbital (see below).

A related case of identical transition energies occurs in ^{153}Dy - the first case where excited superdeformed bands were reported [49]. Here, two excited bands have been interpreted as signature partners and the averages of the transition energies in the partners reproduce the γ-ray energies in ^{152}Dy within 1-3 keV. Finally, the two superdeformed bands of ^{147}Gd have been related to the yrast superdeformed bands of ^{146}Gd and ^{148}Gd respectively, although the average ΔE_γ are somewhat larger in this case (~5 keV) [42]. In the case of ^{147}Gd, another relation applies as well: one of the bands has γ-ray energies following closely (1-4 keV) the average of two successive transition energies in ^{148}Gd, while the other band shows the same property when compared with the superdeformed band of ^{146}Gd.

3.3 Strong Coupling and Identical Bands

The first attempt at an explanation of this surprising phenomenon was presented in refs. [38,54]. The interpretation is done within the framework of the strong coupling limit of the particle-rotor model in which one or more particles are coupled to a rotating deformed core and follow the rotation adiabatically. We note that for rotors the γ-ray energy for a I → I-2 transition is given by:

$$E_\gamma = \frac{\hbar^2}{2\mathcal{J}}[4I-2] \qquad \text{Eq. (1)}$$

If the Coriolis force causes alignment i of the particle along the rotation vector $\underline{R}$, giving R = I-i,

$$E_\gamma = \frac{\hbar^2}{2\mathcal{J}} [4(I-1) - 2] \qquad \text{Eq. (2)}$$

Eq. (2) shows that odd and even nuclei can have identical transition energies if i = 1/2, when $\mathcal{J}^{odd} = \mathcal{J}^{even}$. In the strong coupling limit no alignment is present, i.e. i=0, and the transition energies in an odd nucleus, relative to those in an even-even core, obey simple relations [11] which are shown in fig. 9. Here the moments of inertia for all cases are assumed to be identical. When $K \neq 1/2$, it is seen (fig. 9 (a-c)) that

$$1/2\ [E_\gamma\ (R+1/2) + E_\gamma\ (R-1/2)]_{odd} = E_\gamma\ (R)_{even}$$

This strong coupling relation provides a straightforward explanation for the (^{153}Dy*, ^{152}Dy) pair. The two excited bands in ^{153}Dy have been interpreted [26,49] as a ^{152}Dy⊗ν[514]9/2 structure with no signature splitting -the relevant single-particle levels for protons and neutrons at large deformation are presented in fig. 3 of ref. [55].

For a K = 1/2 band, the transition energies in the odd-nucleus are affected by the decoupling parameter, a, and obey the relation:

$$E_\gamma = \frac{\hbar^2}{2\mathcal{J}} [4I-2 + 2(-1)^{I+1/2}\ a\ \delta_{K,1/2}]$$

The transition energies for a = ±1 are indicated in fig. 9(d-e). Transitions from both signatures form degenerate doublets, with the a = 1 case giving energies identical to those of the core, while the a = -1 case has energies mid-way between those of adjacent transitions in the core. The alignment in a K = 1/2 band is given by $i = (-)^{I-1/2} a/2$.

The three pairs (A-1*,A) where identical energies have been observed can be interpreted as a case where a = 1. In each case, the (A-1)* configuration is A⊗ν([301]1/2)$^{-1}$. If the decoupling parameter a is calculated from the Nilsson wave function of the [301]1/2 orbital, a value of 0.85 is obtained [54] very close to, but not exactly 1. On the other hand, for a [Nn$_3$ Λ]Ω orbital, the decoupling parameter can be calculated from the asymptotic quantum number, by

$$a = (-)^N\ \delta_{\Lambda,0}\ .$$

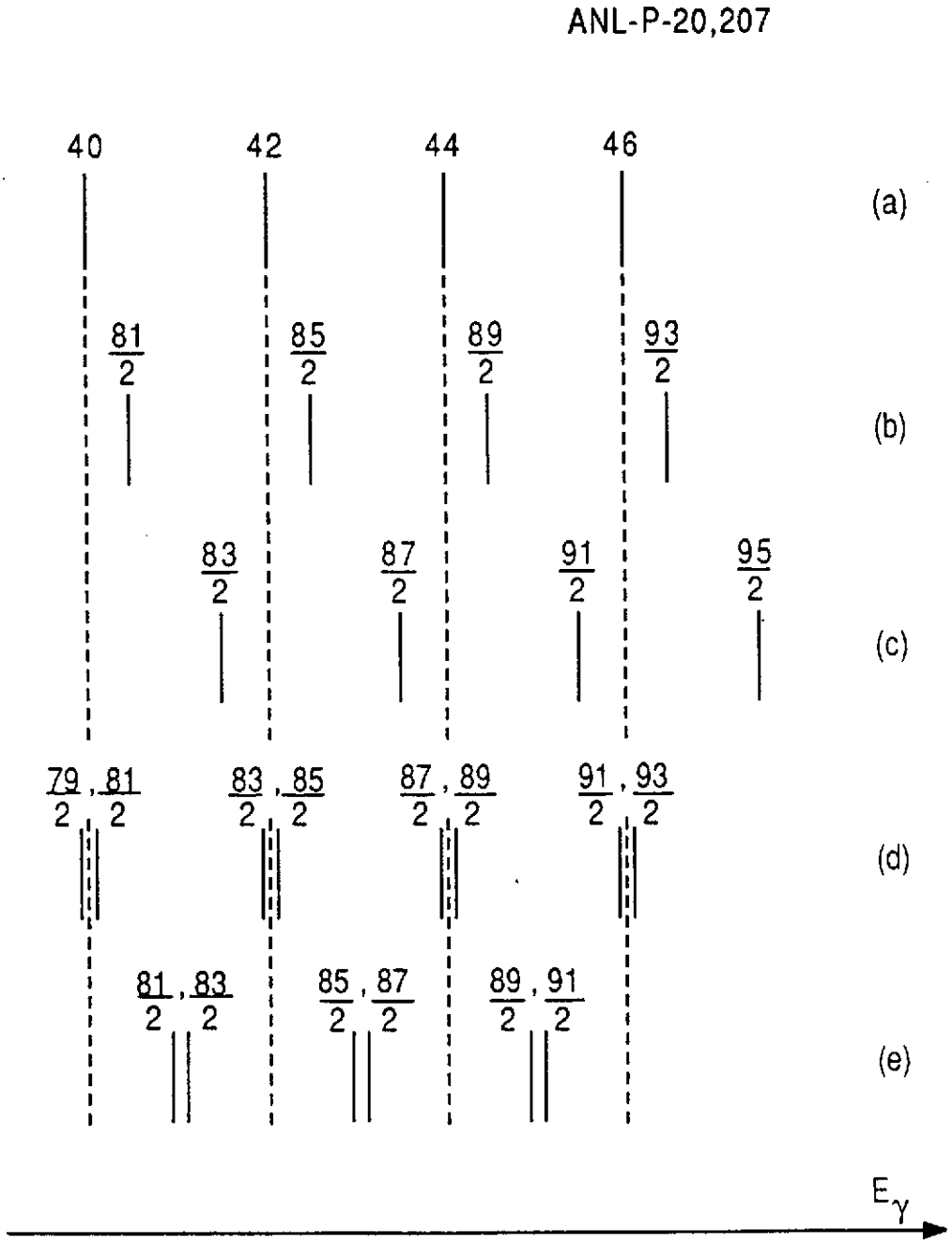

Figure 9: γ-ray energies for transitions in a perfect rotor, assuming identical moments of inertia in all cases: (a) even core; (b) and (c) odd-even nucleus in the strong coupling limit; (d) and (e) odd nucleus with K = 1/2, a =+1 and a = -1, respectively. Note that (d) and (e) also apply for an odd nucleus with alignment $\pm$ 1/2, i.e. I = R $\pm$ 1/2.

which would result in a = 0 for the [301]1/2 orbital. However, if one employed a different coupling scheme in terms of pseudo-spin (see below), the appropriate quantum numbers are [200]1/2, and

$$a = (-)^{\tilde{N}} \delta_{\tilde{\Lambda},0} = 1,$$

providing a natural explanation for the identical energies of the three pairs. A case where a = -1 has not been seen so far, although it is predicted [38,54] within the pseudo-spin scheme to apply an excited superdeformed band in ^{151}Dy, but has not yet been observed.

It must be stressed again that the explanation of identical energies presented here follows only if the moments of inertia for odd and even nuclei are identical. $A^{5/3}$ scaling would give differences of ~1%, as mentioned above. Thus, it still is a puzzle why the moments of inertia J for adjacent nuclei appear to be constant to within ~0.2%.

3.4 Pseudo-spin in Rotating Deformed Nuclei

A simplified analysis of nucleonic motion and of the effect of deformation can be made [56-59] within the framework of the pseudo-spin scheme. In heavy nuclei, this formalism is based on the fact that a major shell, labelled by the total quantum number N, consists of the members of an oscillator shell modified by the removal of the state with largest j(= N+1/2) and the addition of an intruder orbital with opposite parity and j = N+3/2. The remaining normal parity orbitals form close-lying doublets with quantum numbers ℓ_1, $j_1 = \ell_1+1/2$ and $\ell_2 = \ell_1+2$, $j_2 = \ell_2-1/2 = j_1+1$. Examples are the $(d_{5/2},g_{7/2})$ and $(f_{7/2},h_{9/2})$ doublets. The doublets can be relabelled in terms of pseudo quantum numbers $\tilde{\ell} = \ell_1+1$, $\tilde{N} = N-1$. Thus, the doublets $(d_{5/2},g_{7/2})$ and $(f_{7/2},h_{9/2})$ become $\tilde{f}$ and $\tilde{g}$, respectively. A deformed potential preserves this degeneracy: in a Nilsson diagram close-lying nearly parallel orbits are observed as function of deformation (see, e.g. fig. 1 in ref. [59]). The pair of orbits

$$[Nn_3\Lambda,\ \Omega = \Lambda+1/2] \text{ and } [Nn_3\Lambda+2,\ \Omega = \Lambda+3/2]$$

can be relabelled with pseudo quantum numbers

$$[\tilde{N} = N-1,\ n_3,\ \tilde{\Lambda} = \Lambda+1,\ \Omega = \tilde{\Lambda} \pm 1/2].$$

This doublet can be viewed as pseudo-spin-orbit partners. The important feature is that the $\tilde{\ell}\cdot\tilde{s}$ interaction is substantially smaller than the normal $\ell\cdot s$ coupling. Since the $\tilde{\ell}\cdot\tilde{s}$ coupling is weak, the Coriolis force readily causes $\tilde{s}$ to align along the rotation vector, i.e. $\tilde{s}_1 = \pm 1/2$. One sees, therefore, that pseudo-spin can lead to $i = 1/2$ in equation (2) and account for identical transition energies in odd and even nuclei by offsetting the intrinsic spin difference of $1/2\hbar$ [60].

The case for $K = 1/2$ bands has been discussed above, where it was pointed out that the pseudo-spin formalism naturally provides the correct decoupling parameter for explaining bands with identical transition energies. For orbits with $K \neq 1/2$, the alignment in an odd nucleus relative to an even core will, in general, have non-zero contributions from alignment $\tilde{\ell}_1$ of the pseudo orbital angular momentum [59]. (Only if $\tilde{\ell}_1 = 0$ will one obtain the simple spectrum given in fig. 9(d-e). Thus, it will not be easy to find experimental evidence for pseudo-spin alignment by comparing data in odd and even nuclei for orbits with $K \neq 1/2$. However, Hamamoto [61] has suggested that evidence for pseudo-spin alignment may be found in an alignment difference of $1\hbar$ for pairs of orbits which constitute doublets with identical $\tilde{\ell}_1$ and $\tilde{s}_1 = \pm 1/2$ (see also Figs. 3 and 4 in ref. [59]). Examples of such doublets have so far not been identified. Detection of those doublets will probably require detection of more (weak) excited superdeformed bands, as well as firm spin assignments.

3.5 Identical Moments of Inertia

The identical bands discussed above require moments of inertia J in different nuclei to be equal to a remarkable degree. Since J depends on several factors (mass, deformation, polarization effects, alignment and pairing) the equality in J is very striking and leads one to wonder about the possibility of a fundamental explanation. The standard models are unable to reproduce transition energies with an accuracy of ~1 keV. We note that only a few identical bands are observed among the many superdeformed bands in this region and that three of these pairs of bands involve a common orbital. This suggests that the phenomenon is associated with only a few specific orbitals. Indeed, it is recognized that occupation of different high-N intruder orbits will not result in identical bands because the orbital energies tend to have steep slopes as a function of both deformation and rotational frequency, i.e. strong polarization and alignment effects will result. Ragnarsson [62] has

used a simple harmonic oscillator model to show that for particles or holes in certain orbitals there can be cancellation among the different terms contributing to changes in J. He has been able to reproduce the "identical" energies observed in (^{152}Dy, ^{153}Dy*), where the orbital occupied in ^{153}Dy* is either ν[402]5/2 or ν[514]9/2. These orbitals slope upward with increasing β_2 - so-called oblate orbitals - so that a particle here would tend to decrease the deformation of the (A+1) nucleus, compensating the increase in J due to the larger mass. Agreement for other cases calculated by Ragnarsson, including that involving the π[301]1/2 hole (responsible for the three pairs of bands with identical energies) is not as satisfactory, suggesting that other effects, such as changes in pairing, should be included. A further requirement for the orbital is that the alignment be small, a criterion satisfied by the "oblate" orbitals.

4. IDENTICAL BANDS IN THE A = 190 REGION

4.1 Identical Transition Energies and Relation to ^{192}Hg

There are even more examples of identical superdeformed bands in the A = 190 region [63,64]. However, two features distinguish the bands in this region from those near A = 150: (a) many of the bands occur in pairs separated by two mass units and (b) a large number of bands can be related to the superdeformed band in ^{192}Hg, which appears to serve as a doubly-magic core. These features are illustrated in fig. 10a, which shows the degree of similarity between transition energies in the pairs [^{191}Hg(2), ^{193}Hg(2)], [^{191}Hg(3),^{193}Hg(3)], [^{192}Hg,^{194}Hg(3)] and [^{192}Hg,^{194}Pb]. [The numbers in brackets () correspond to the labels given to different bands in the original publications and numbers larger than 1 designate excited bands]. Figure 10b relates transition energies of ^{192}Hg to those of bands in adjacent nuclei ^{191,193}Hg and ^{193}Tl through the relationship:

$$\Delta E^*_\gamma = 1/2\ [E^f_\gamma(R\pm1/2) + E^u_\gamma(R\mp1/2)] - E^{core}_\gamma(R),$$

where R is the core angular momentum, and u and f designate transitions from favored and unfavored states in signature partner bands of the odd-even nucleus. As discussed in ref. [64] and in section 2 above, the proposed configurations for these superdeformed bands are characterized by $K \neq 1/2$. As a result both features in fig. 10 can be understood in a straightforward way in the strong coupling scheme, which gives $\Delta E^*_\gamma = 0$. However, there is again the requirement of equal moments of inertia in all nuclei.

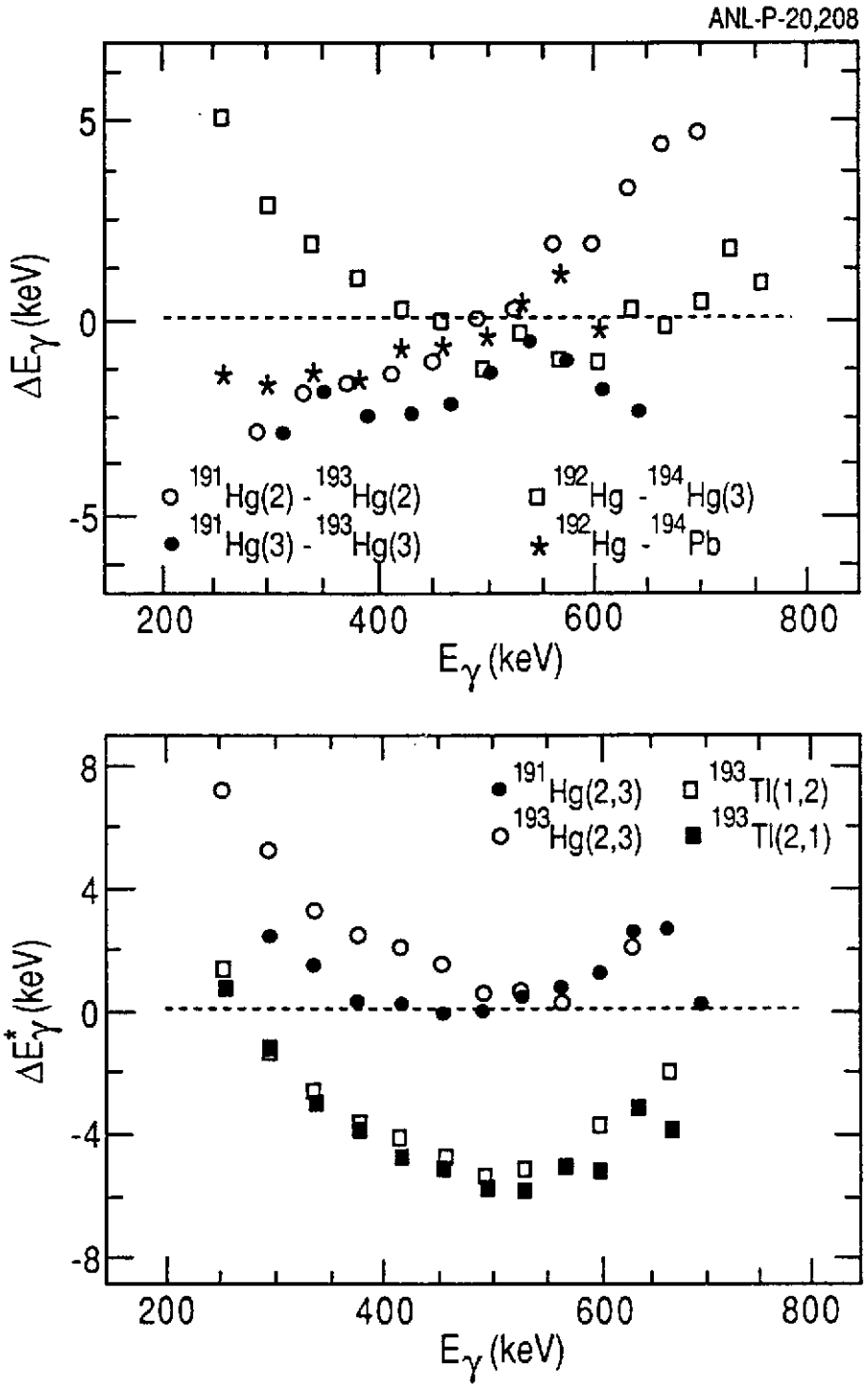

Figure 10: (a): Difference in transition energy ΔE_γ, between selected superdeformed bands in the A = 190 region region.
(b): Energy difference ΔE^*_γ (see text) referenced to ^{192}Hg for strongly coupled bands in ^{191,193}Hg and ^{193}Tl. For both (a) and (b), the data are from ref. [21-23,28,34] (from ref. [64]).

Another way of relating the energies of different bands to those of a reference, ^{192}Hg, has been proposed by Stephens et al [63], using the quantity

$$\Delta i = 2 \frac{\Delta E_\gamma}{\Delta E_\gamma^{ref}},$$

where $\Delta E_\gamma = E_\gamma - E_\gamma^{ref}$ is obtained by subtracting the transition energy E_γ in a band of interest from the closest transition energy in ^{192}Hg (E_γ^{ref}), and ΔE_γ^{ref} is calculated as the energy difference between the two closest transitions in the reference. Δi has been called incremental alignment in ref. [63], but is not necessarily related to any physical alignment. In the strong coupling limit, $\Delta i = \pm 1/2$ for an odd nucleus referred to an even core, as can readily be seen in fig. 9a-c. For even nuclei, bands with the same or different signatures have $\Delta i = 0$ or 1, respectively. Plots of Δi are shown in fig. 11, which illustrates that the superdeformed bands of the A = 190 region can be classified in two families. When additional particles (holes) with respect to ^{192}Hg occupy lower K members of the high-N intruder orbitals, values of Δi scatter significantly (fig. 11a). This is not surprising since particles in these intruder orbitals tend to both increase deformation and align with rotation, thus making the strong coupling scheme inappropriate. In contrast, when the orbitals involved do not show much variation with $\hbar\omega$ (see fig. 4), i.e. when there is little alignment, Δi values fall close to the limits of 0, $\pm$ 1/2, $\pm$1, which are expected in the strong coupling limit (fig. 11b).

Stephens et al [40,63] suggested that many of the cases which exhibit Δi = 0, $\pm$1/2, or $\pm$1 also have integer alignment differences with respect to the core, which they refer to as quantized alignment. While the strong coupling limit corresponds to a zero alignment difference, ref. [40] instead suggests alignments (with respect to ^{192}Hg) of $1\hbar$ in, for example, ^{191}Hg (2,3) and ^{194}Hg(2,3), which are then attributed to pseudo-spin alignment. An alignment of $1\hbar$ in ^{191}Hg, instead of the expected $1/2\hbar$, is not easy to understand. However, a word of caution is in order. Whereas extraction of Δi does not require knowledge of spin, determination of alignment does. So far the spins of superdeformed band members have not been assigned using the conventional, tested techniques of γ-ray spectroscopy. Methods to infer the spin have been suggested [23,65,66], and are discussed below. At present, it is not established whether these methods give the exact spin or have uncertainties of at least $1\hbar$ [67,68]. Thus, until spins can be assigned firmly, one cannot

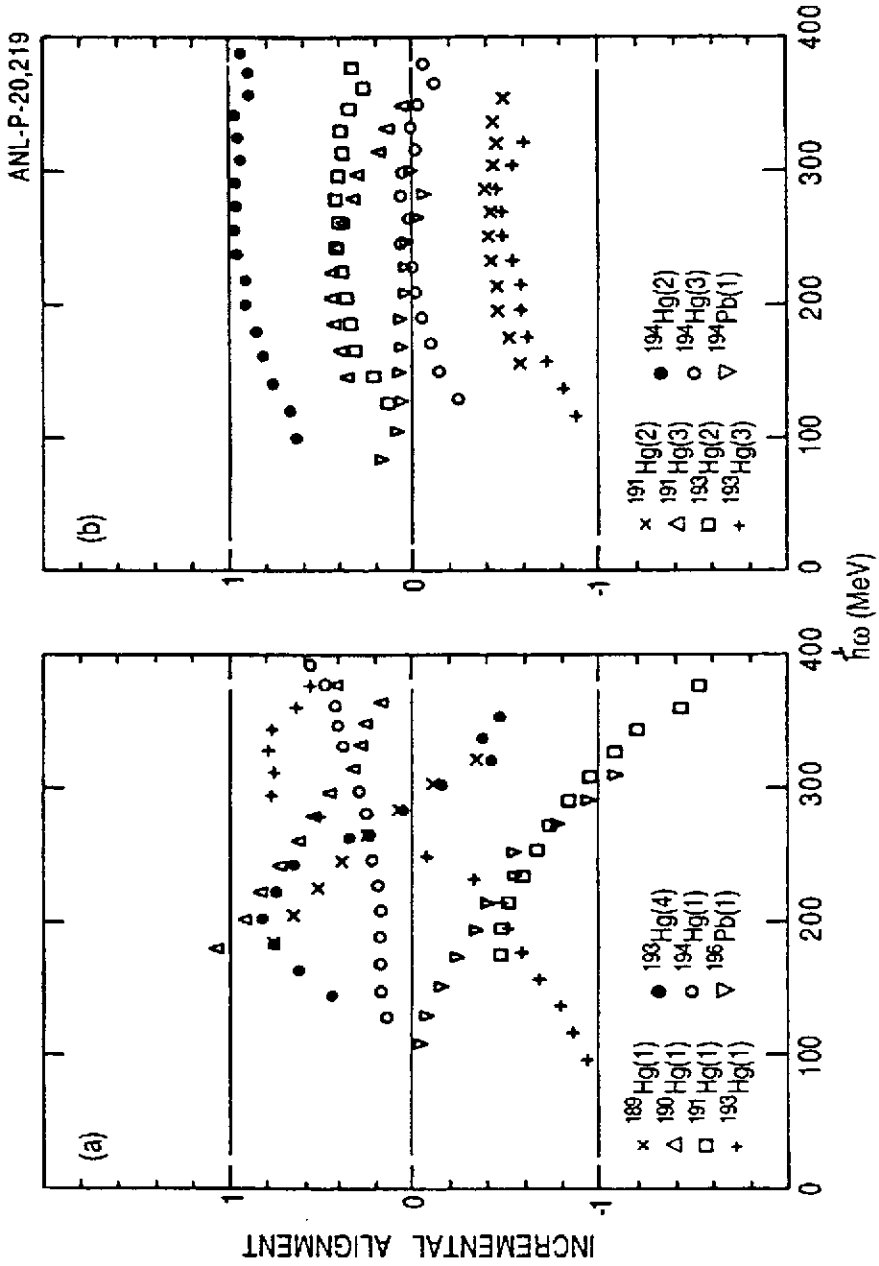

Figure 11: Incremental alignment Δi as a function of rotational frequency for superdeformed bands in $^{189-194}$Hg [21-23,28-33] and ^{194,196}Pb [36,37], with ^{192}Hg as a reference. As discussed in the text, the data are grouped [(a) and (b)] in order to illustrate the existence of two families; in (b) Δi clusters around integer and half-integer values. The data on superdeformed bands in the Tl isotopes have been omitted for clarity; these are discussed in ref. [35].

be certain whether the alignments have the putative value of $1\hbar$ [40] or simply have the value $0\hbar$ expected from strong coupling.

4.2 Spin Assignments

Several related procedures for assigning spins to superdeformed states in the A = 190 region have been proposed recently [23,65,66]. These procedures all start from a Harris expansion [69] of the moment of inertia

$$\mathcal{J}^{(2)} = J_0 + J_1\omega_x^2 + \ldots$$

and the relation

$$\frac{dI_x}{d\omega_x} = \mathcal{J}^{(2)} \qquad \text{Eq. (3)}$$

where I_x is the projection of spin along the rotation vector, and $\omega_x = \Delta E_\gamma/\Delta I_x$ is the corresponding rotational frequency. Integrating Eq. 3 gives

$$I_x = J_0\omega + \frac{J_1}{3}\omega^3 + i_0 \qquad \text{Eq. (4)}$$

where i_0 is the constant of integration. The parameters J_0 and J_1, obtained by fitting $\mathcal{J}^{(2)}$ as a function of ω_x, are used to determine I_x with Eq. 4. The spin I is then derived from the relation

$$I_x = \sqrt{I(I+1) - K^2}\ ,$$

where K is the projection of angular momentum along the symmetry axis. It has been shown [70] that reasonable choices of K do not sensitively affect the derived spin. Two assumptions need to be valid for the derived spin to be correct. First, it must be assumed that the fit of $\mathcal{J}^{(2)}$ vs ω can be correctly extrapolated to zero frequency. (A minimal requirement for this assumption to be correct is that $\mathcal{J}^{(2)}$ varies smoothly and gradually in the low frequency domain.) Second, the constant of integration i_0, which corresponds to the alignment at zero frequency, must be known. It has been assumed in ref. [65,66] that $i_0 = 0$, since this results in calculated values of I which are within $0.1\hbar$ of the integer or half-integer value appropriate for an even or odd-nucleus. However, it has not been unambiguously demonstrated that both assumptions are valid. In fact, pairing may well change as $\hbar\omega$ approaches

zero, leading to uncertainty in the extrapolation of $J^{(2)}$, and resulting in an "effective" alignment (i.e. an effect which mimics alignment). The extent to which these effects are subsumed into the parameters J_o and J_1 is not clear. Other attempts at spin determination [67,68] have concluded that spin uncertainties of at least 1$\hbar$ exist. Thus, there is a clear need to determine the actual spins of superdeformed band members experimentally in order to resolve these uncertainties.

4.3 Strong Coupling Limit and Identical Moments of Inertia

In the discussion above it was suggested that the identical bands can be understood in terms of the strong coupling limit of the particle-rotor model, with the additional requirement that the moments of inertia be identical. The following questions must then be raised: why does this strong coupling limit work so well and why are the moments of inertia so close? These are interesting questions for theory to address quantitatively, but qualitative comments can be made at this point. As discussed in section 3.3, the strong coupling limit applies when the alignment is zero. (Assuming equal J values for the bands, the identical energies suggest $i \lesssim 0.1\hbar$.) At the large deformations discussed here, alignment effects are expected to be small: the large value of the moments of inertia and the increased separation between Nilsson levels from a given shell both reduce the Coriolis coupling which is responsible for the alignment. In addition, the reduced pairing discussed in section 2 also leads to less alignment. These qualitative arguments, however, do not guarantee that $i \lesssim 0.1\hbar$ -as implied by the equal transition energies- and, indeed, cranked shell model calculations [70] suggest that alignments of the order of $\sim 0.5 - 1\hbar$ are obtained.

It has been emphasized above that identical transition energies require equal moments of inertia in the bands. This feature is unexpected since the masses involved differ by as much as two units. In the A = 190 region, scaling by $J \sim A^{5/3}$ results in a ~ 5 keV difference per mass unit. Furthermore, bands are compared where the number of quasiparticles associated with the superdeformed configurations differ by one or two. These bands can be expected to have different moments of inertia J because blocking may be present which reduces pairing. A major question remains whether the equality of the moments of inertia reflects some hitherto undiscovered symmetry.

Another interesting observation can be added. When $\mathcal{J}^{(2)}$ values for all the known superdeformed bands in the A = 190 region are compared (see fig. 5), they are all found to cluster within $\lesssim$10% (with the exception of 4 cases). This is indeed a surprise since bands which differ by 0, 1 or 2 quasiparticle excitations are included. For rotational bands at normal deformation, $\mathcal{J}^{(2)}$ values increase by ~15% per quasiparticle because of reduced pairing due to blocking. One wonders if the reduced pairing in superdeformed bands, which is partially responsible for smaller alignment, is also responsible for the noted clustering in $\mathcal{J}^{(2)}$ values.

5. OTHER IMPORTANT EFFECTS AT LARGE DEFORMATION

Some pairs of orbitals such as the $i_{13/2}$-$f_{7/2}$ and the $j_{15/2}$-$g_{9/2}$ orbitals which are responsible for strong octupole correlations in light actinide nuclei [71] also appear close to the Fermi level in superdeformed configurations around ^{152}Dy and ^{192}Hg. Several recent calculations [32,72-75] have indicated that for many superdeformed nuclei the minima in the total energy surfaces exhibit considerable octupole softness which is expected to persist even at the highest spins. As a result, collective octupole vibrational excitations can be mixed with low-lying one- and two-quasiparticle states and the excitation pattern near the superdeformed yrast line can be different from that expected for axial symmetry. The calculations suggest that the first excited state in the doubly-magic superdeformed nuclei ^{152}Dy and ^{192}Hg should be of collective octupole character and an analogy can be drawn with the well-known collective 3^- state in the doubly-magic spherical nucleus ^{208}Pb. Octupole correlations are also expected to reduce single-particle alignments, increase band interactions, and modify the deexcitation pattern of the superdeformed states because of enhanced B(E1) rates [71]. Most of the anticipated effects still remain to be observed experimentally. However, first evidence for strong mixing of quasiparticle excitations with octupole vibrations may have been seen in ^{193}Hg [32]. In this nucleus, two of the four superdeformed bands are characterized by moments of inertia $\mathcal{J}^{(2)}$ strikingly different from those of all other superdeformed bands in this region (see fig. 5), i.e. one shows a strong upbend at the frequency where the other shows a strong downbend. Furthermore, there is indirect experimental evidence for enhanced E1 transitions linking one of the irregular bands with the yrast superdeformed band. These observations, together with the reduced alignments observed and the strong interaction between the crossing bands, have been interpreted as evidence for strong octupole correlations [32]. In

the mass A = 150 region, one of the proposed explanations for the behavior of one of the superdeformed bands in ^{147}Gd invokes collective octupole excitations [42,76] as well, but other interpretations are also possible [46].

It has been suggested recently [77] that the residual n-p interaction may also play a role in superdeformed nuclei. Such an interaction is expected to be strong in situations where protons and neutrons occupy rotationally aligned high-N intruder orbitals with large spatial overlap, such as the $\pi i_{13/2}$ and $\nu j_{15/2}$ orbitals involved in the superdeformed bands of the A = 150 and 190 regions. Such an interaction is expected [77] to lower the energy of superdeformed bands based on these specific intruder configurations with respect to other excitations in the superdeformed well. Firm experimental evidence for the importance of this interaction is currently lacking even though it has been invoked to explain the strong feeding of a superdeformed band in ^{142}Eu [51] (interaction between N=6 odd proton and odd neutron) and the smooth rise of $J^{(2)}$ with $\hbar\omega$ in the lighter Hg isotopes (interaction between 4 N=6 protons and 4 N=7 neutrons) [30].

6. FEEDING AND DECAY OF SUPERDEFORMED BANDS

Superdeformed bands are populated to much higher spins than states with smaller deformation (referred to as "normal" states hereafter) and have about an order of magnitude larger intensity than might be expected from the intensity pattern of the normal states [10,78]. These features make it interesting to try to understand the population mechanism. Important elements affecting the feeding are the level densities of both normal and superdeformed states, the mixing between the two classes of states at moderate excitation energy, the electromagnetic decay rates in the normal and superdeformed minima [78,79], as well as the barrier separating the two minima [80]. Thus, investigations of the feeding mechanism also yield information on these aspects, providing perhaps the main incentive for such studies. Furthermore, knowledge of this mechanism allows selection of optimal conditions (in terms of reaction and bombarding energy) for spectroscopic studies of superdeformation.

Insight on the feeding mechanism may be obtained from data for both superdeformed and normal states on: (a) population intensities as a function of spin and beam energy for one or several projectile-target combinations; (b) distributions in spin and energy at entry into the final nucleus; (c) shapes

of the quasicontinuum and statistical spectra associated with the feeding of the two classes of states; and (d) the properties of ridge structures in E_γ-E_γ correlation matrices. Unfortunately, data on this problem have not kept pace with the steady flow of information on the many superdeformed bands discussed above. Only (a) and (b) are discussed here (see ref. [81] for a discussion of (c), ref. [10,79] for a discussion of (d)).

6.1 Intensities of Superdeformed Bands

Figure 12 presents, as a function of the rotational frequency $\hbar\omega$, the relative intensities of transitions in ^{149}Gd and ^{192}Hg, which are representative of superdeformed nuclei in their respective regions. In the A = 150 region, the number of coincident γ rays is generally larger and the transition energies are almost twice as large. The latter is principally due to the larger spins of the emitting states and, to a lesser extent, to the smaller moments of inertia. The first and last transitions in the superdeformed bands in ^{149}Gd and ^{192}Hg correspond to estimated spins of (63/2, 131/2$\hbar$) and (10, 42$\hbar$), respectively [44,22,23]. In both cases, the population extends to much higher spin than in the normal states. Figure 12 also shows another similarity between bands in the two regions: as the spin decreases, the intensity gradually increases, flattens out at the maximum and then drops rapidly within a couple of transitions as the bands decay to the lower-lying normal states. The superdeformed bands are weakly populated in all cases, with maximum intensities reaching about 1 and 2% in the A = 150 and A = 190 regions, respectively.

6.2 Entry Distributions

The entry distribution, representing the population distribution in spin and excitation energy after neutron emission, can be measured for superdeformed and normal states with 4π detector calorimetric arrays which, together with Compton-suppressed Ge detectors, constitute the detection systems used in all superdeformation studies. Data on complete distributions have not been published, but information exists on the average entry points, i.e. the centroids of the distributions. The latter have been derived from data on the total energy and fold (average number of detectors firing) measured in coincidence with discrete normal or superdeformed transitions. The entry points for normal and superdeformed states in ^{192}Hg, measured at several bombarding energies with the ^{160}Gd(^{36}S,4n) reaction, are given in

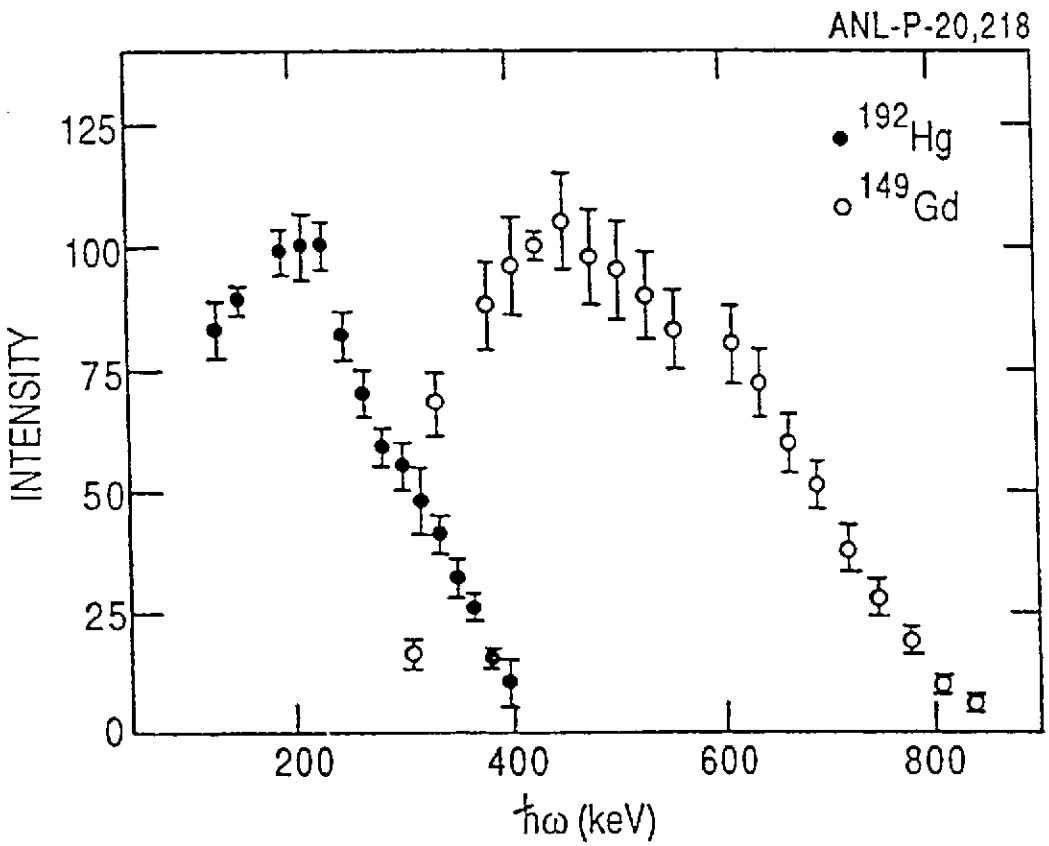

Figure 12: Relative intensities as a function of frequency $\hbar\omega$ for ^{192}Hg [22] and ^{149}Gd [44], normalized to 100 at their respective maxima.

Fig. 13(a) [80]. The entry spins for the superdeformed states are higher than those for the normal states and the initial population leading to superdeformed states is colder, i.e. the entry points are lower in excitation energy than those of normal states at the same spin. Similar data on entry points for the A = 150 region have not been published, but the sum-energy and fold for normal and superdeformed states in ^{149}Gd have been measured [82] (Fig. 13(b)). As spin scales approximately linearly with fold, Fig. 13(b) shows that feeding of superdeformed bands also originates from higher spin and lower energy, as for ^{192}Hg. Thus, feeding of superdeformed bands in both A = 150 and A = 190 regions share common characteristics.

Since the entry spins for ^{149}Gd must necessarily be larger than the average spin where the discrete superdeformed band is fed (~ 111/2$\hbar$), the spins of the states from which the superdeformed bands originate are larger in ^{149}Gd than in ^{192}Hg. On the other hand, the maximum angular momenta brought into the compound nuclei are comparable in the two cases. The lower entry spin in ^{192}Hg is attributed [80] to the depletion of the highest partial waves by fission, which predominates over evaporation residue formation beyond spin 40$\hbar$. (Thus, superdeformed bands have been identified in this nucleus near to the limit of fission instability.) It is striking that the feeding of the superdeformed bands originates from the highest spins in the evaporation residues. This occurs because the level densities of superdeformed states exceed that of the normal states only for the highest spin.

Schiffer and Herskind [78,79] have performed an extensive series of calculations, which successfully described many of the observed feeding features in ^{152}Dy and which have provided insight into the population mechanism. The calculations start by describing the first phase of the decay of the compound nucleus, i.e. neutron evaporation and fission, to obtain an entry distribution in spin and energy from which γ decay occurs. The decay is then followed through Monte Carlo simulations and consists of a competition at each step between electromagnetic decay (E1 statistical γ decay, which cools the nucleus, and collective E2 γ decay, which removes two units of angular momentum) in the normal and superdeformed wells, and hopping between the normal and superdeformed wells. It was found to be important that, as the energy increases, the level density for the superdeformed states increases less rapidly than for the normal states. This results in a limited region in excitation energy where the density of superdeformed states is larger than that of normal states. This region corresponds to the highest partial waves

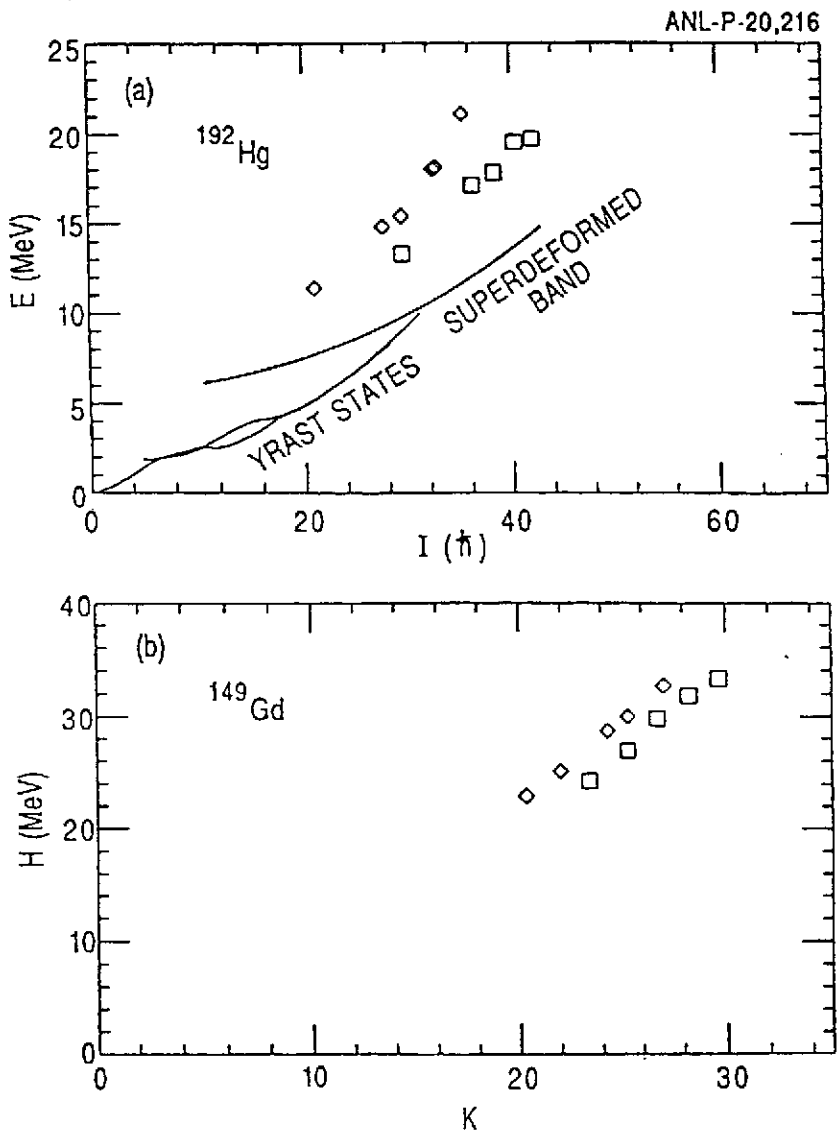

Figure 13: (a): Entry points for normal (diamonds) and superdeformed (squares) states in ^{192}Hg measured in the ^{160}Gd(^{36}S,4n) reaction at several bombarding energies [80]. The known yrast states are indicated; the energy of the superdeformed band is not known and is arbitrarily chosen.
(b): Average sum-energy H and fold K for normal and superdeformed states in ^{149}Gd measured at a number of projectile energies in the ^{124}Sn(^{30}Si,5n) reaction [82].

and is located roughly beyond the point where the superdeformed band crosses the normal states and becomes yrast (Fig. 13). Schiffer and Herskind suggest that the entry states for the superdeformed band originate from this region and that this feature accounts for the "colder" feeding of the superdeformed bands. Although the barrier between the superdeformed and normal states was included in the calculations and governed the tunnelling between the two wells, its role is not emphasized. It has been proposed in ref. [80] that the the barrier may, in fact, play the pivotal role since mainly entry states within the superdeformed well (i.e. states which are below the barrier) are likely to be trapped within the well. If this is indeed the case, then the entry energy is closely related to the barrier energy. As a result, a measurement of the entry points could provide a determination of the barrier and also of the superdeformed well depth, although the latter requires knowledge of the excitation energy of the band. These quantities are directly related to the shell correction which is responsible for the superdeformed pocket and, thus, are interesting to compare with theoretical values.

6.3 Deexcitation of Superdeformed Bands

The sudden decrease of superdeformed transition intensities at low frequencies (Fig. 12) indicates that, after a long cascade of consecutive intraband transitions, a rapid decay towards the lower-lying normal states takes place. So far, none of the decay paths linking the superdeformed bands with the normal states has been identified in the A = 150 or 190 regions, suggesting that the decay is fragmented into many pathways, each too weak to define, and is probably statistical in nature [78]. It has, therefore, not been possible to define the spins and excitation energies of superdeformed band levels with standard spectroscopic techniques. This task remains the major open challenge in the study of superdeformation.

The transition from a superdeformed to a normal shape represents a large amplitude motion involving a drastic structural rearrangement. It is perhaps not surprising that the decay is fragmented into many intermediate excited states involving, in some cases, a time delay before the yrast line is reached [21,83].

The deexcitation of superdeformed bands represents an interesting problem which has been addressed by a number of recent calculations [78,84,85]. As γ decay occurs within a superdeformed band, a curious situation occurs where the

excitation energy of the superdeformed states with respect to the yrast levels increases (see Fig. 13a). At the point of decay, the superdeformed levels have an estimated energy of 3-6 MeV above yrast. Hence, a cold state, isolated within its own potential well, is immersed in a hot sea of normal states with very high density. The decay then occurs through admixtures with this sea of states. Properties of the decay, e.g. the spin dependence of the out-of-band decay probability, can provide information on the mixing between the superdeformed and normal states and on the barrier separating them. The gross energy distribution of the decay γ rays may also provide additional information. (It may be possible to determine this distribution more easily than to trace out the individual pathways.)

7. SUMMARY AND OUTLOOK

Superdeformed nuclei have now been discovered in four distinct regions of the periodic table with masses around A=130, 150, 190 and 240, and with respective axis ratios of 3:2, 1.9:1, 1.7:1 and 2:1. These coincide with the regions where theory, which incorporates a macroscopic liquid drop term and a quantal shell-correction term, also predict the occurrence of nuclei with very large deformation. This success represents a triumph for the Strutinsky method, and for mean-field theories in general, in describing the macroscopic and microscopic aspects of nuclear behavior.

In the A=150 and 190 regions, which have been reviewed here, it has been possible to perform spectroscopic studies in the superdeformed secondary well, and both "ground" and excited bands have been observed. An unexpected discovery is that a number of the excited bands have energies identical to those of the lowest superdeformed bands in adjacent nuclei. The degeneracies of better than one part in 500 require that the moments of inertia be identical and also that the strong coupling limit applies, both to a remarkable degree. It is not clear whether this is a result of an accident or is a consequence of a symmetry which has yet to be identified. Perhaps models which exploit symmetries, such as the interacting model [86], may shed light on this question. One also wonders if the identical energies of bands in even and odd nuclei might be a manifestation of supersymmetry [87], which covers both fermion and boson degrees of freedom. Pseudospin alignment partially accounts for identical energies in superdeformed bands of some adjacent even and odd nuclei, but it is not clear if it plays a significant role in other identical bands.

Although there has been much progress in research on superdeformation, many questions remain and, indeed, have actually been raised by the new discoveries. Certainly, a major challenge is to determine the excitation energies and spins of superdeformed levels since there is not a single superdeformed band in the A=150 and 190 regions for which these properties are known. The borders of the regions of superdeformation in the periodic table need to be established. The known excited superdeformed bands are believed to correspond to particle or quasiparticle excitations, but the collective modes associated with states of large deformation, e.g. the beta, gamma or octupole vibrations are yet to be found. If the deformation is stiff with respect to quadrupole distortion, the beta vibrations may lie at high excitation energies, but soft octupole modes may exist at lower energies [88], possibly giving rise to exotic bending modes. To shed more light on the cause of identical bands, it will probably be necessary to identify higher-lying particle states to, for instance, search for evidence of pseudo spin-orbit doublets and pseudospin alignment, as described in Section 3.4.

Investigations of the mixing between states in the normal and superdeformed well will give information on the barrier separating them and on the superdeformed well-depth. Both quantities are important to study as they are direct manifestations of the shell-corrections leading to the formation of the superdeformed pocket. Mixing in excited states can be investigated through the properties of ridges in the E_γ-E_γ matrices and, at higher energies, by studying the feeding mechanism of superdeformed bands. Finally, mixing between cold superdeformed states and excited normal ones can be studied through the decay properties involved in the deexcitation out of superdeformed bands.

At present experiments are limited by the detection capabilities of current γ-ray detectors. The next generation detector arrays currently under construction (GAMMASPHERE in the USA and EUROGAM in Europe) will improve the detection sensitivity by about two orders of magnitude and provide answers to the questions raised above. Many fascinating discoveries about superdeformation -- and about nuclear structure in general -- lie ahead.

Acknowledgments

The data and ideas reviewed above are the result of dedicated work by many colleagues and friends. It is impossible to name them all here. We would like, however, to acknowledge the contributions of our collaborators at Argonne, Notre Dame, Purdue, I.N.E.L., Stockholm and Warsaw. We also thank Mike Carpenter, Patricia Fernandez and Frank Moore for carefully reading the manuscript. This work was supported by the Department of Energy, Nuclear Physics Division, under contract no W-31-109-ENG-38.

References:

1. Strutinsky, V.M., Nucl. Phys.A95:420-42(1967);A122:1-33(1968)
2. Polikanov, S.M., et al., Sov. Phys. JETP15:1016-21(1962)
3. Tsang, C.F., Nilsson, S.G., Nucl. Phys.A140:275-288(1970)
4. Bengtsson, R., et al., Phys. Lett.57B:301-5(1975)
5. Ragnarsson, I., et al., Nucl. Phys.A347:287-315(1975);A347:287-315(1980)
6. Dudek, J., Nazarewicz, W., Phys. Rev.C31:298-301(1985)
7. Chasman R.R., Phys. Lett.187B:219-23(1987)
8. Twin, P.J., et al., Phys. Rev. Lett.57:811-4(1985)
9. Kirwan, A.J., et al., Phys. Rev. Lett.58:467-70(1987)
10. Nolan, P.J., Twin, P.J., Ann. Rev. Nucl. Part. Sci.38:533-62(1988)
11. Bohr, A., Mottelson, B.R., Nuclear Structure,vol. 2: Benjamin, Reading, Mass., (1975)
12. Nilsson, S.G., et al., Nucl. Phys.A131:1-66(1969)
13. Åberg, S.,Phys. Scr.25:23-7(1982)
14. Bengtsson, T., Ragnarsson I., Nucl. Phys.A436:14-82(1985)
15. Chasman, R.R., Phys. Lett.219B:227-31(1989).
16. Girod M., et al., Phys. Rev. Lett.62:2452-6(1989)
17. Bonche, P., et al., Nucl. Phys.A500:308-22(1989)
18. Moore, E.F., et al., Phys. Rev. Lett.63:360-3(1989)
19. Nazarewicz, W., et al., Phys. Lett.255B:208-14(1989)
20. Bengtsson, T., et al., Phys. Lett.208B:39-43(1988)
21. Riley, M.A., et al., Nucl. Phys.A512:178-88(1990)
22. Ye, D., et al., Phys. Rev.C41:R13-6(1990)
23. Becker, J.A., et al.,Phys. Rev.C41:R9-12(1990)
24. Hubel, H., et al., Nucl. Phys.A453:316-48(1986)
25. Moore, E.F., et al., Phys. Rev. Lett.64:3127-30(1990)
26. Nazarewicz, W., et al., Nucl. Phys.A503:285-330(1989)
27. Bengtsson T., Nucl. Phys.A496:56- (1989)
28. Carpenter M.P., et al. Phys. Lett.240B:44-9(1990)
29. Janssens, R.V.F., et al.,Nucl. Phys.A520:75c-90c(1990)
30. Drigert, M.W., et al.,Nucl. Phys. in press
31. Henry E.A., et al., Z. Phys.A335:361-2(1990)
32. Cullen, C.M., et al., Phys. Rev. Lett.65:1547-50(1990)
33. Beausang, C.W., et al., Z. Phys.A335:325-30(1990)
34. Fernandez, P.B., et al. Nucl. Phys.A517:386-98(1990)
35. Azaiez, F., et al., Z. Phys.A336:243-4(1990); Phys. Rev. Lett.66:1030-3(1991)

36. Brinkman, M.J., et al., Z. Phys.A336:115-6(1990)
37. Theine, K., et al., Z. Phys.A336:113-4(1990)
38. Nazarewicz, W., Proceedings XXV Zakopane School on Physics, to be published
39. Chasman, R.R., Phys. Lett.242B:317-22(1990)
40. Stephens, F.S., et al., Phys. Rev. Lett.64:2623-6(1990);65:301-4(1990)
41. Hebbinghaus, G., et al., Phys. Lett.240B:311-6(1990)
42. Zuber, K., et al., Nucl. Phys.A520:195c-200c(1990) and to be published
43. Deleplanque, M.A., et al., Phys. Rev. Lett.60:1626-9(1988)
44. Haas, B., et al., Phys. Rev. Lett.60:503-6(1988); Phys. Rev.C42:R1817-21(1990)
45. Fallon, P., et al., Phys. Lett.218B:137-42(1989); and to be published
46. Janzen, V.P., et al., Proceedings Int. Conf. on High Spin Physics and Gamma-soft Nuclei, to be published
47. Deleplanque, M.A., et al., Phys. Rev.C39:1651-4(1989)
48. Rathke, G.-E., et al.,Phys. Lett.209B:177-81(1988)
49. Johansson, J.K., et al.,Phys. Rev. Lett.63:2200-3(1989)
50. Lieder, R.M., et al.,Nucl. Phys.A520:59c-66c(1990)
51. Twin, P.J, Nucl. Phys.A520:17c-33c(1990) and Mullins S.M., et al., to be published
52. Shimizu, Y.R., et al., Phys. Lett.198B:33-3(1989); Nucl. Phys.A509:80-116(1990)
53. Byrsky, T., et al., Phys. Rev. Lett.60:503-7(1990)
54. Nazarewicz, W., et al.,Phys. Rev. Lett.64:1654-8(1990)
55. Twin, P.J., Nucl. Phys.A522:13c-30c(1991)
56. Hecht, K.T. and Adler, A., Nucl. Phys.A137:129-43(1969)
57. Arima, A., et al., Phys. Lett.30B:517-22(1969)
58. Ratna-Raju R.D., et al., Nucl. Phys.A202:433-66(1973)
59. Bohr, A., et al., Phys. Scr.26:267-72(1982)
60. Mottelson, B., Nucl. Phys.A520:711c-22c(1990)
61. Hamamoto, I., private communication and to be published
62. Ragnarsson, I., Nucl. Phys.A520:67c-74c(1990)
63. Stephens, F.S., Nucl. Phys.A520:91c-104c(1990)
64. Satula, W. et al., Nucl. Phys. in press
65. Becker, J.A. et al., Nucl. Phys.A520:188c-94c(1990
66. Draper, J.E., et al., Phys. Rev. C42:R1791-5(1990)
67. Wu, C. et al., to be published
68. Wyss, R., Pilotte, S., to be published
69. Harris, S.M., Phys. Rev.B509:138-54(1965)

70. Carpenter, M.P., et al., to be published
71. Nazarewicz, W., Nucl. Phys.A520:333c-51c(1990) and references therein
72. Höller, J., Åberg, S., Z. Phys.A336:363-4(1990)
73. Åberg, S., Nucl. Phys.A520:35c-57c(1990)
74. Dudek, J. et al., Phys. Lett.248B:235-42(1990)
75. Bonche, P. et al., to be published
76. Szymanski, Z.,Nucl. Phys.A520:1c-16c(1990)
77. Wyss, R., Johnson, A.,Proceedings Int. Conf. on High Spin Physics and Gamma-soft Nuclei, to be published
78. Herskind, B., Schiffer, K., Phys. Rev. Lett.59:2416-9(1987)
79. Schiffer, K., et al., Z. Phys.A332:17-27(1989)
80. Khoo, T.L., et al.,Nucl. Phys.A520:169c-77c(1990)
81. Moore, E.F., et al., Proceedings Workshop on Nuclear Structure and Heavy-ion reaction Dynamics, Inst. Phys. Conf. Ser. 109:171-8(1991)
82. Taras, P. et al., Phys. Rev. Lett.61:1348-51(1988) and Haas, B. et al, Phys. Lett.B245:13-6(1990)
83. Carpenter, M. P., et al.,Nucl. Phys.A520:133c-7c(1990)
84. Vigezzi, E., et al., Phys. Lett.B249:163-7(1990)
85. Bonche, P., et al., Nucl. Phys.A519:509-20(1990)
86. Iachello, F., Arima, A., The Interacting Boson Model, Cambridge Univ. Press, Cambridge (1987) and Iachello, F., Nucl. Phys.A522:83c-98c(1991)
87. Iachello, F., van Isacker, P., The Interacting Boson Fermion Model, Cambridge Univ. Press, Cambridge (1990)
88. Mizutori, S., et al., to be published